공학박사 학위논문

Cell-derived Nanovesicles for Cancer Immunotherapy

세포 유래 나노소포체를 이용한 암 면역치료

2023 년 8 월

서울대학교 대학원

협동과정 바이오엔지니어링

홍 지 혜

Cell-derived Nanovesicles for Cancer Immunotherapy

지도 교수 김 병 수

이 논문을 공학박사 학위논문으로 제출함
2023 년 8 월

서울대학교 대학원
협동과정 바이오엔지니어링
홍 지 혜

홍지혜의 공학박사 학위논문을 인준함
2023 년 8 월

위 원 장 황 석 연 (인)

부위원장 김 병 수 (인)

위 원 정 연 석 (인)

위 원 조 장 환 (인)

위 원 심 가 용 (인)

Abstract

Keyword: cancer, cancer immunotherapy, nanovesicles, T cell therapy, cancer vaccines
Student Number: 2018-25874

Unlike previous cancer therapies, cancer immunotherapy utilizes patient's own immune system, inducing antitumor activity of immune cells. Currently, cancer vaccines, adoptive T cell therapy and immune checkpoint inhibitors are the most prominent cancer immunotherapies, showing remarkable clinical outcomes. However, these immunotherapies still have obvious limitations, such as immune escape of tumor cells and difficulty in target antigen identification. Therefore, here I suggest cell-derived nanovesicles as a novel cancer immunotherapy. T cell-derived nanovesicles (TCNVs) and senescent cancer cell-derived nanovesicles (SCCNVs) preserve characteristics of parental cells, and they successfully induced proper immune response in vitro and in vivo, resulting in impressive antitumor efficacy in mice tumor models. Taken together, cell-derived nanovesicles offer an effective cancer immunotherapy strategy to overcome current limitations of cancer immunotherapy.

Table of Contents

List of Figures

Chapter 1. Introduction

1.1. Study Background

1.1.1. Overview of cancer immunotherapy

Cancer is a life-threatening disease worldwide, being the second leading cause of death in US in 2020.[1] There has been a continuous development of novel cancer therapy, and chemotherapy, radiotherapy, and surgery have been the most standard-of-care treatments to cancer patients. Then, D. Jim Allison at The University of Texas MD Anderson Cancer Center, has been awarded the 2018 Nobel Prize in Physiology or Medicine for developing a novel way to attack cancer cells by modulating the immune system rather than the tumor, which is now called cancer immunotherapy.[2] Cancer immunotherapy has opened the new era of cancer treatment, and several clinical outcomes showed a potential way to overcome cancer.

Cancer immunotherapy, such as adoptive T cell therapy, immune checkpoint blockade therapy and cancer vaccination activates antitumor immunity in cancer patients and has shown significant success in clinical oncology.[3-6] However, despite of successful clinical outcomes of these immunotherapeutics, there are still limitations that impede proper treatment of cancers. Therefore, there are countless efforts to understand immune system and tumor cell-immune cell interaction in tumor microenvironments.

1.1.2. Activation of immune system

Briefly, activation of immune system requires antigen uptake and presentation of antigen presenting cell (APC)s, migration of T cells to tumor tissues and cytolytic activity of $CD8^+$ T cells toward tumor cells. Therefore, many researchers tried to modulate each step, facilitating immune cells to detect and properly attack tumor cells. Representative immunotherapies against cancer are introduced below.

1.1.3. Cancer vaccine adjuvant and neoantigens

Antigen uptake and presentation is the first step in immune activation. APCs, representatively dendritic cells and macrophages, scavenge pathogens and cellular debris, and present antigens to T cells. Therefore, for the proper activation of T cells, APCs must be properly maturated and be able to present appropriate antigens to T cells. To enhance antigen presentation, several studies have tried to deliver tumor antigens with adjuvants to APCs, such as CpG, Poly I:C, and R848[7]. These TLR agonists can be recognized by TLRs of APCs, and induce downstream inflammatory signals. Thus, while immunogenicity of antigens may vary between antigens, addition of these adjuvants can improve efficiency of antigen presentation by APCs. Moreover, in addition to vaccine adjuvants, there are some trials to improve quality of antigens presented by APCs. Neoantigens, which is usually identified by whole-exome sequencing, are only expressed in tumor cells, therefore lowers the risk of on-target off-tumor side effects and induce tumor specific immune response[8].

1.1.4. Adoptive T cell therapy

In adoptive T cell therapy, T cells are isolated from patient blood and modified ex vivo, to artificially infuse tumor attacking T cells. There are several T cell modification methods, such as TIL isolation, TCR modification or chimeric antigen receptor (CAR) modification.[9] Among these methods, CAR-T therapy showed significant clinical outcomes. CAR-T cells have chimeric antigen receptor, therefore when they recognize tumor antigens, downstream activation signaling domain activates CAR-T cells to attack tumor cells. With enhanced antigen specific tumor recognition, CAR-T therapy showed impressive efficacy against liquid tumors.[10] In Liquid tumors, such as B cell acute lymphoblastic leukemia, multiple myeloma and B-cell non-Hodgkin lymphoma, CAR-T infusion successfully inhibited tumor progression with high response rates.

1.1.5. Immune checkpoint inhibitors

Immune checkpoints are surface receptor of immune cells, which can turn-on or -off the immune responses. These immune checkpoints exist to prevent over-activation of immune cells, but these checkpoints can be used as tumor escape routes, inducing immune suppression of T cells. Therefore, antibody that blocks immune checkpoints was used to protect immune cells from tumor mediated immune suppression. Clinically approved immune checkpoint inhibitors are anti-programmed cell death protein-1 (PD-1) antibody, anti-programmed death-ligand 1 (PD-L1) antibody, anti-cytotoxic T-lymphocyte-associated protein 4 (CTLA-4) antibody and lastly anti-lymphocyte-activation gene 3 (LAG-3) antibody.[11] These antibodies can block immune checkpoints on T cells and support activation of T cells, and showed impressive clinical outcomes with higher survival rates and complete remission of tumors in some patients.

1.1.6. Cell-derived nanovesicles for cancer immunotherapy

Cell-derived nanovesicles are nano-sized vesicles from serial extrusion of cells, and these vesicles possess exosome mimetic characteristics. First suggested by Jang and his collegues[12], these vesicles contain larger amounts of RNAs and proteins than naturally obtained exosomes, and preserve parental cells' cellular characteristics. With higher yield and easier production procedure than natural exosomes, these cell-derived nanovesicles are getting attention for a potential nanotherapeutic.

Currently, there are already several clinical trials to test exosomes to treat various diseases, such as pneumonia, sepsis and other inflammatory diseases[13]. While there is no clinical trial testing cell-derived nanovesicles, nanovesicles can resolve devastating yield of exosome production, and MDimune Inc, a novel biotechnology company, is planning clinical applications of cell-derived nanovesicles[14].

Moreover, cell-derived nanovesicles are advantageous as drug carrier nanoplatforms. As they possess parental cell's membrane receptors and signaling proteins, they can be utilized to target specific tissue and cells and also non-immunogenic[15]. This enhanced targeting ability without further modification is highly desirable as drug carriers, which is hard to achieve in synthetic nanocarriers such as liposomes.

1.2. Purpose of Research

While these cancer immunotherapies showed remarkable clinical success in some cancer patients, still there are many hurdles to overcome. For instance, CAR-T cells showed limited efficacy in solid tumors partly due to immune suppressive tumor microenvironment. For tumor antigen presentation, there are continuous mutations in tumor tissues and heterogeneity among tumor cells, which makes difficult to identify exact target antigen. Moreover, improving immunogenicity of tumor antigens is needed to induce proper immune responses.

Here, I propose cell-derived nanovesicles to improve current cancer immunotherapy. Cell-derived nanovesicles are produced by serial extrusion of cells, exhibit exosome-like phenotypes. These cell-derived nanovesicles preserve parental cells' characteristics, including RNAs and proteins, and therefore various cell-derived nanovesicles have been developed as therapeutics, such as mesenchymal stem cells[16].

Therefore, I suggest T cell-derived nanovesicles (TCNVs) and senescent cancer cell-derived nanovesicles (SCCNVs) as potential antitumor therapeutics. TCNVs are produced from activated $CD8^+$ T cells, and they preserve surface proteins of $CD8^+$ T cells. TCNVs modulate tumor microenvironments by three mechanisms: 1) blocking PD-L1 on tumor cells 2) scavenging (Transforming growth factor-beta) TGF-β in tumor

microenvironments and 3) granzyme B mediated tumor suppression. These three antitumor mechanisms simultaneously act in tumor microenvironments, boosting T cell's antitumor activity. SCCNVs, produced from senescence induced cancer cells, deliver cancer cell antigens with pro-inflammatory cytokines as adjuvants. SCCNVs showed improved antigen presentation and dendritic cell maturation, resulting in significant tumor suppression in several tumor models.

Chapter 2. T-cell-derived nanovesicles for cancer immunotherapy

2.1. Introduction

Adoptive T cell therapy, the infusion of T cells into patients after ex vivo expansion, has shown a remarkable success in clinical cancer treatment. Especially, CAR-T cell therapy, which uses T cells genetically engineered to express a tumor antigen-recognizing receptor, has shown impressive therapeutic outcomes in patients with hematological malignancies.[17-19] Adoptively transferred T cells recognize cancer cells and kill the cells by delivering potent cytotoxic molecules such as granzyme B.[20] However, T cell therapy including CAR-T cell therapy has shown limited efficacy for solid tumors, partly due to cancer cell-mediated exhaustion of T cells in the immunosuppressive solid tumor microenvironment (TME).[21,22] The exhaustion is caused mainly by PD-L1 and TGF-β in the solid TME.[23] PD-L1 on cancer cells induces cytotoxic T cell exhaustion via PD-L1/ PD-1 interactions, resulting in decreased secretion of pro-inflammatory cytokines and low cytolytic activity against cancer cells.[24] Cancer cells and regulatory T (Treg) cells in TME secrete TGF-β, which induces T cell exhaustion.[25-27] TGF- β downregulates anti-tumor activity of cytotoxic T cells and induces differentiation into anti-inflammatory immune cells, including M2 macrophages and Treg cells, in TME, eventually accelerating immune suppression of cytotoxic T cells.[28,29]

To overcome these limitations, here I developed TCNVs. TCNVs were produced from activated $CD8^+$ T cells (Figure 2.1A). TCNVs preserve cytotoxic T cell membrane proteins (e.g., PD-1 and TGF-βR) and intracellular granzyme B, both of which are contained in activated cytotoxic T cells. TCNVs aid cytotoxic T cells to eliminate cancer cells by reversing the immunosuppressive TME and directly killing cancer cells (Figure 2.1B). PD-1 and TGF-βR on TCNVs can interact with PD-L1 on cancer cells and TGF-β in TME, respectively, preventing PD-L1- or TGF-β-mediated exhaustion of $CD8^+$ T cells.[24,30] In addition, TCNVs directly induce cancer cell apoptosis by delivering granzyme B to the cancer cells. Unlike T cells that are vulnerable to the immunosuppressive molecule-mediated exhaustion and subsequently lose their cytotoxic functions, TCNVs maintain their anti-tumoral activity even in the immunosuppressive TME. In this study, I evaluated the ability of TCNVs to rescue T cells from exhausted states and directly induce cancer cell apoptosis. Next, I examined whether TCNVs inhibit tumor growth in syngeneic solid tumor-bearing mice. Furthermore, I investigated whether TCNVs maintain their anti-tumoral capacity in PD-L1- and TGF-β-rich environment.

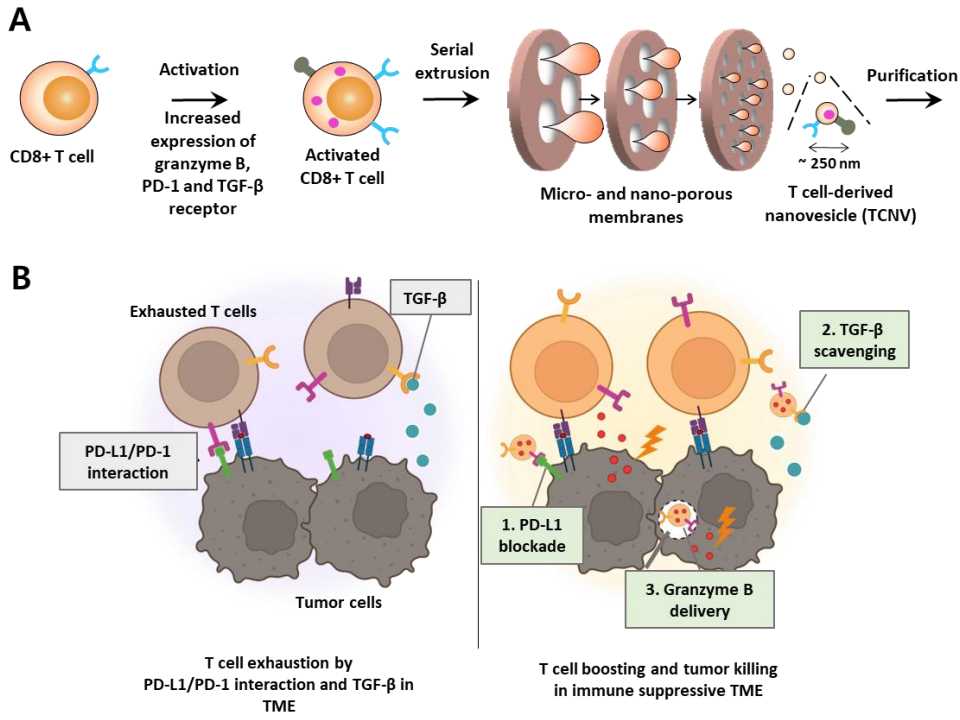

Figure 2.1 Preparation, anti-cancer mechanisms and characterization of TCNVs.

A) Schematic illustration of TCNV preparation. **B**) Schematic illustration of mechanisms of TCNV-mediated tumor eradication. Created from Biorender.com

2.2. Results and Discussion

2.2.1. Characterization of TCNVs

TCNVs were prepared from activated OVA-specific $CD8^+$ T cells (OT-1 $CD8^+$ T cells) by serial extrusion through polycarbonate membranes with pore sizes of 1 μm, 400 nm and 200 nm (Figure 2.1A). OT-1 $CD8^+$ T cells were efficiently expanded ex vivo using ovalbumin peptides and interleukin-2 (IL-2). A transmission electron microscopic image of TCNV revealed an unilamellar structure with lipid bilayers (Figure 2.2A). Dynamic light scattering analysis revealed that the hydrodynamic diameter of TCNVs is approximately 249.2 nm (Figure 2.2B). Electrophoretic light scattering analysis showed that the zeta-potential of TCNVs is -23.0 mV and that the zeta-potential of activated T cells is preserved in TCNVs (Figure 2.2C). Flow cytometric analysis showed that PD-1, TGF-βR and granzyme B, which are highly expressed upon T cell activation,[31,32] were preserved in TCNVs prepared from activated T cells. (Figure 2.2D). Trypsinized TCNVs (trTCNVs) lost PD-1, TGF-βR and granzyme B. TCNVs were stable in serum-containing fluid at least for a week and showed no significant change in the particle diameter (Figure 2.2E).

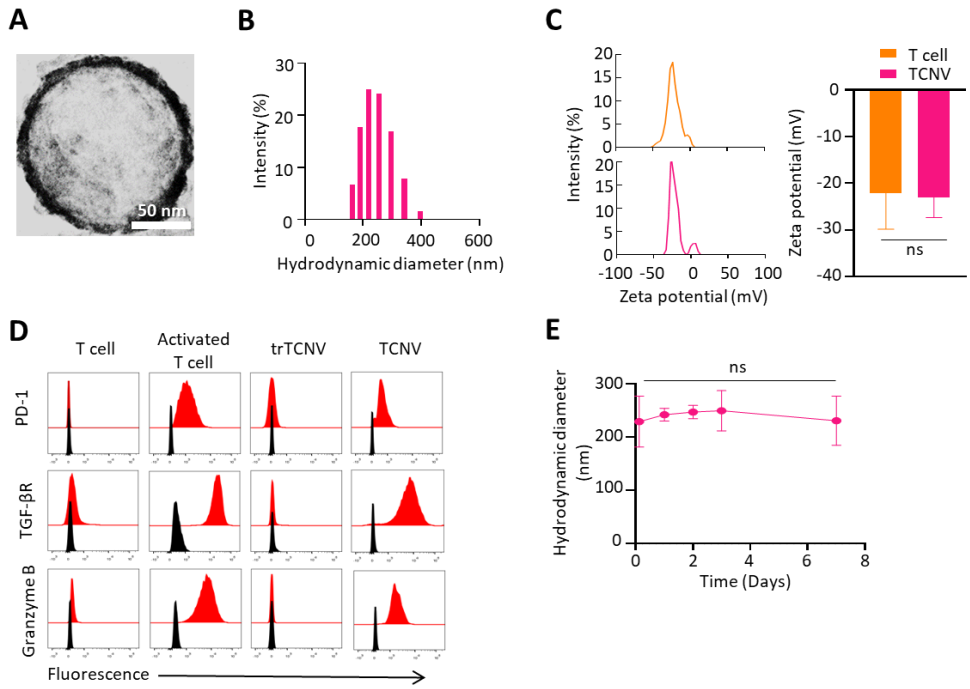

Figure 2.2 Characterization of TCNVs.

A) Transmission electron microscopic image of TCNV. **B)** Size distribution and **C)** zeta potential of TCNVs. **D)** Flow cytometric analysis showing that PD-1, TGF-β receptor (TGF-βR) and granzyme B were maintained on TCNVs produced by the serial extrusion of activated T cells. Black peaks show fluorescence intensity of isotype control. trTCNV: trypsinized TCNV. **E)** Hydrodynamic diameter of TCNVs incubated in 10 % (v/v) serum-containing buffer for various time periods, showing stability of TCNVs. n = 3. ns = not significant.

2.2.2. In vitro test of TCNVs as PD-L1 blockade

To determine whether PD-1 on TCNV can block PD-L1 on cancer cell surface, TCNV binding to cancer cells was investigated (Figure 2.3A). Anti-PD-L1 antibody treatment to TCNVs hampered the TCNV binding to cancer cells, indicating a significant portion of the TCNV binding is mediated by PD-1/PD-L1 interactions between TCNVs and cancer cells. This result suggests that TCNVs can be used to inhibit PD-1/PD-L1 interaction-mediated T cell exhaustion by interfering interactions between PD-1 on T cells and PD-L1 on cancer cells. trTCNVs showed less binding to cancer cells, likely due to the deletion of the membrane proteins including PD-1, indicating the membrane proteins on TCNVs mediate the TCNV binding to cancer cells. Importantly, TCNV treatment to $CD8^+$ T cells in vitro effectively inhibited PD-1/PD-L1 interaction-mediated exhaustion of $CD8^+$ T cells, maintaining T cell cytotoxicity against cancer cells (Figure 2.3B). PD-1-blocked TCNVs (PbTCNVs) failed to inhibit the PD-L1-mediated exhaustion of $CD8^+$ T cells, demonstrating that PD-1 on TCNVs is responsible for the inhibition of T cell exhaustion by TCNVs.

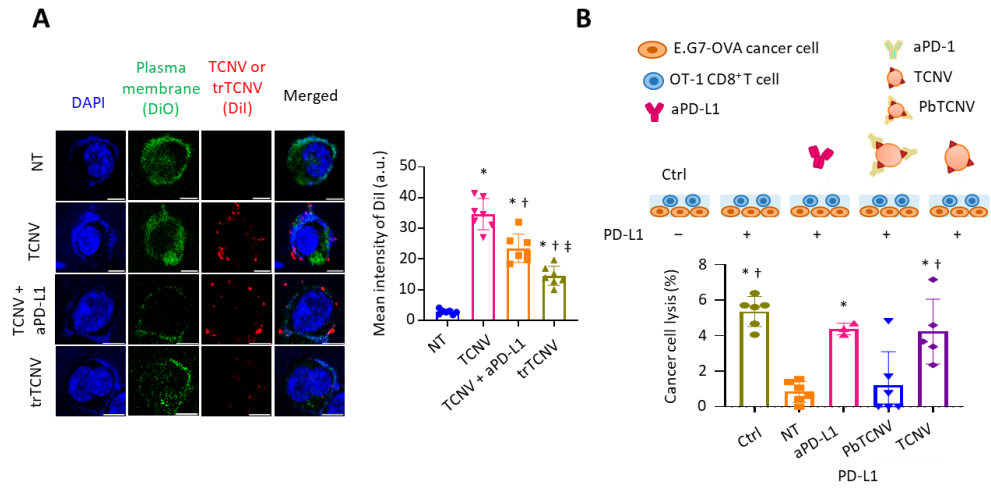

Figure 2.3 PD-L1 blocking by TCNV in vitro.

A) Representative confocal fluorescence microscopic images and quantification of mean intensity of DiI, showing that LLC cancer cell interacts with TCNVs through cell membrane proteins such as PD-L1 after 2 hrs of treatment. aPD-L1: anti-PD-L1 antibody. Scale bars = 10 μm. n = 7. **B**) Rescue of PD-L1-mediated T cell exhaustion by TCNVs in cocultures of cancer cells and T cells. Cancer cell death in the cocultures was evaluated by LDH assay. aPD-L1: anti-PD-L1 antibody. aPD-1: anti-PD-1 antibody. PbTCNV : PD-1-blocked TCNV. n = 3-6. Statistic analysis was calculated by one-way analysis of variance (ANOVA) with Tukey's significant difference multiple comparisons. * $P < 0.05$ versus NT. † $P < 0.05$ versus TCNV in (A); versus PbTCNV in (B). ‡ $P < 0.05$ versus TCNV + aPD-L1 in (A).

2.2.3. In vitro test of TCNVs as TGF−β scavenger

Next, I investigated whether TCNVs can scavenge TGF-β, a major cytokine produced by cancer cells, and reduce T cell cytotoxicity in a TGF-β-rich immunosuppressive environment. Enzyme-linked immunosorbent assay (ELISA) showed that TCNVs can successfully scavenge TGF-β in vitro, as the residual TGF-β concentrations in the TCNV-treated group were significantly lower than those in the TGF-βR-blocked TCNV (TbTCNV)-treated group (Figure 2.4A). To determine whether TCNV can inhibit TGF-β-mediated immune suppression, cytotoxicity of $CD8^+$ T cells against tumor cells was evaluated by lactate dehydrogenase (LDH) assay in vitro. TGF-β-mediated T cell exhaustion was effectively blocked by TCNVs, as the T cell cytotoxicities against cancer cells were not different between the TGF-β + TCNV group and TGF-β + aTGF-β group (Figure 2.4B). The TGF-β + TbTCNV group showed lower cytotoxicity, demonstrating that TGF-βR on TCNVs is responsible for the inhibition of T cell exhaustion by TCNVs.

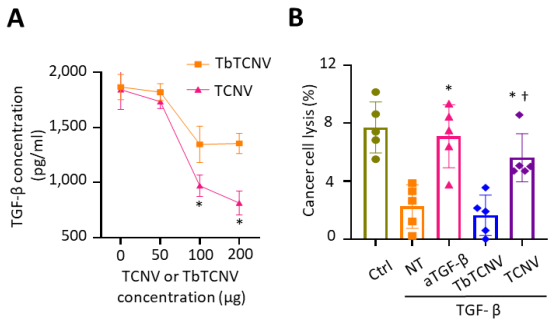

Figure 2.4 TGF-β scavenging by TCNV in vitro.

A) Residual TGF-β concentration after TbTCNV or TCNV treatment, as determined by ELISA assay, showing that TCNV scavenges TGF-β. TbTCNV : TGF-βR-blocked TCNV. n = 4. **B)** Rescue of TGF-β-mediated T cell exhaustion by TCNV in cocultures of cancer cells and T cells. Cancer cell death in the cocultures was evaluated by LDH assay. The Ctrl (control) indicates no TGF-β. aTGF-β: anti-TGF-β antibody. TbTCNV: TGF-βR-blocked TCNV. n = 5. Statistic analysis was calculated by one-way analysis of variance (ANOVA) with Tukey's significant difference multiple comparisons. * $P < 0.05$ versus TbTCNV in (A); versus NT in (B). † $P < 0.05$ versus TbTCNV in (B).

2.2.4, In vitro cytotoxicity of TCNVs to tumor cells

In addition, TCNVs, which contain granzyme B (Figure 1F), can directly kill cancer cells via delivery of granzyme B to cancer cells. Following the TCNV internalization, granzyme B contained in the TCNVs was observed in the cytoplasm of the cancer cells (Figure 2.5A). As determined by qPCR, the mRNA expressions of BID and caspase-9 were upregulated in the TCNV-treated LLC cancer cells (Figure 2.5B), indicating the TCNV-mediated delivery of granzyme B induced the granzyme B-mediated apoptosis pathway in the cancer cells.[33,34] Cancer cell staining with anti-cleaved caspase-3 antibodies revealed that the TCNV treatment induced cleavage of caspase-3 (Figure 2.5C). The TCNV treatment increased annexin V and propidium iodide (PI) double positive cancer cell population in a TCNV dose-dependent manner (Figure 2.5D), demonstrating that TCNV can induce apoptosis of cancer cells through caspase pathway. Taken together, these results demonstrate that TCNVs can directly induce apoptosis of cancer cells.

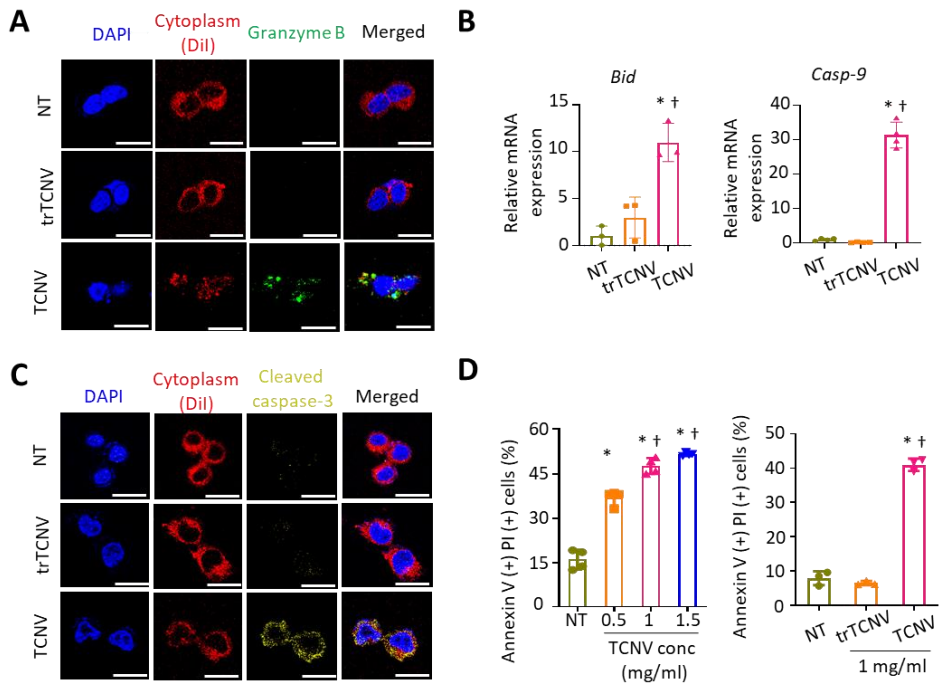

Figure 2.5 Direct delivery of granzyme B by TCNVs in vitro.

A) Fluorescence images showing uptake of granzyme B-containing TCNVs by LLC cancer cells in vitro. Scale bars = 100 μm. **B**) Relative mRNA expression levels of BID and caspase-9 in LLC cancer cells after various treatments in vitro (n = 3-4). **C**) Immunocytochemistry for cleaved caspase-3 in cancer cells (scale bars = 100 μm) and **D**) flow cytometric analysis for evaluation of apoptotic (Annexin V and PI double positive) LLC cancer cells (n = 3) following various treatments in vitro. Statistic analysis was calculated by one-way analysis of variance (ANOVA) with Tukey's significant difference multiple comparisons. * $P < 0.05$ versus NT. † $P < 0.05$ versus trTCNV or 0.5 mg/ml TCNV.

2.2.5. In vivo tumor challenge of TCNVs in lung cancer model

To investigate in vivo anti-tumoral efficacy of TCNVs, TCNVs were intratumorally injected to LLC mouse lung cancer cell-inoculated mice (Figure 2.6A). The injected TCNVs effectively suppressed in vivo tumor growth in comparison with PBS- or trTCNV-injected groups (Figure 2.6B). The TCNV injection significantly prolonged the animal survival (Figure 2.6C). The tumor weight of the TCNV-treated group at day 21 was significantly lighter than those of the other groups (Figure 2.6D). TUNEL staining (Figure 2.6E) of tumor tissues showed significantly higher cancer cell apoptosis in the TCNV-treated group, showing TCNV-mediated anti-tumor effects.

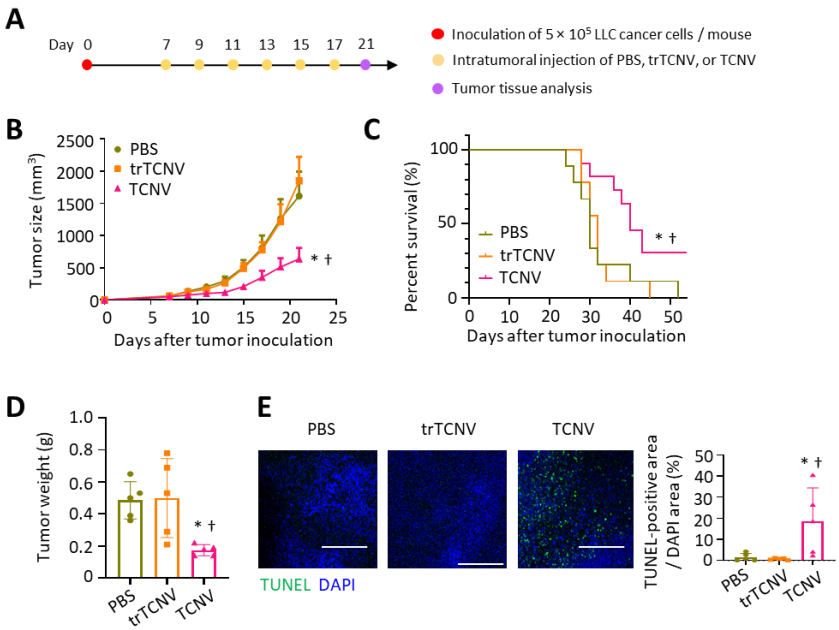

Figure 2.6 Inhibition of in vivo tumor growth by intratumoral injection of TCNV.

A) The LLC tumor modeling in mice and treatment schedule. **B)** Tumor growth profiles in PBS-, trTCNV-, or TCNV-treated mice. n = 8. **C)** Survival rate of the tumor-bearing mice. n = 8. **D)** Tumor weight at day 21. n = 5. **E)** TUNEL staining of the tumor tissues at day 21. Scale bars: 1 mm. n = 3. Data represent mean ± SD. Statistical significance was calculated by log rank (Mantel–Cox) test, one-way ANOVA with Tukey's significant difference multiple comparisons, or by two-way ANOVA with Bonferroni post-tests. * $p < 0.05$ versus PBS; † $p < 0.05$ versus trTCNV.

2.2.6. TCNV mediated tumor microenvironment modulation

To determine whether injected TCNVs rescued $CD8^+$ T cells from exhaustion in the immunosuppressive TME, I conducted tumor infiltrating lymphocyte (TIL) analysis. The TCNV-treated group showed significantly higher cytotoxic function of $CD8^+$ T cells, as revealed by higher expressions of (Tumor necrosis factor) TNF-α, Interferon (IFN)-γ, and granzyme B in the $CD8^+$ T cells in tumors (Figure 2.7A). These results suggest that $CD8^+$ T cells in the TCNV-treated groups were less affected by the suppressive TME, likely due to the PD-1 blockade and TGF-β scavenging by TCNVs as shown in Figure 2.3. Moreover, Treg cell population in the tumors was reduced by the TCNV injection (Figure 2.7B), showing the TCNV injection reversed the immunosuppressive TME. Since TGF-β produced by cancer cells can induce Treg cells in the TME,[25,26] the diminished Treg cell population in the TCNV-treated group may be attributed to TGF-β scavenging by TCNVs and death of TGF-β-secreting cancer cells by TCNVs.

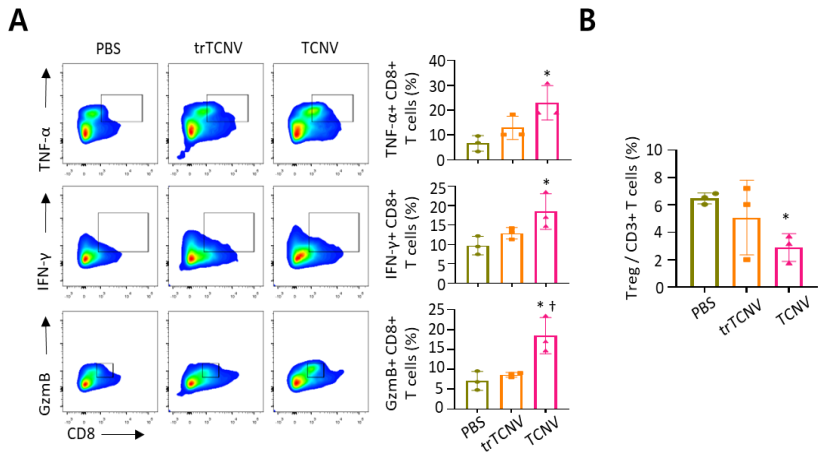

Figure 2.7 Analysis of tumor infiltrating lymphocytes after intratumoral injection of TCNVs.

A) Flow cytometric analysis of tumor infiltrating lymphocytes at day 21. n = 3. **B)** Percentage of Tregs in the tumor infiltrating lymphocytes at day 21. Statistical significance was calculated by one-way ANOVA with Tukey's significant difference multiple comparisons. * $p < 0.05$ versus PBS; † $p < 0.05$ versus trTCNV.

2.2.7. In vivo antitumor efficacy of intravenously TCNVs in lung cancer model

I investigated whether intravenous injection of TCNVs to tumor-bearing mice can eradicate tumor (Figure 2.8A). Ex vivo imaging analysis indicated a significant portion of intravenously injected TCNVs were observed in the tumor tissues 24 hrs after injection (Figure 2.8B). The tumor targeting of TCNVs may be mediated by TCNV surface proteins such as Lymphocyte function-associated antigen 1 (LFA-1)[35-37] and Enhanced permeability and retention (EPR) effects.[38] It is known that LFA-1 on T cell surface interact with inflamed endothelial cells in tumor, contributing to T cell accumulation in tumor.[35-37] Importantly, intravenously injected TCNVs significantly suppressed the tumor growth in LLC tumor-bearing mice compared to the PBS-injected group (Figure 2.8C). TUNEL staining of the tumor tissue sections showed apoptosis of cancer cells was induced by the TCNV injection (Figure 2.8D), demonstrating TCNV-mediated prevention of cytotoxic T cell exhaustion and/or direct killing of cancer cells by TCNVs.

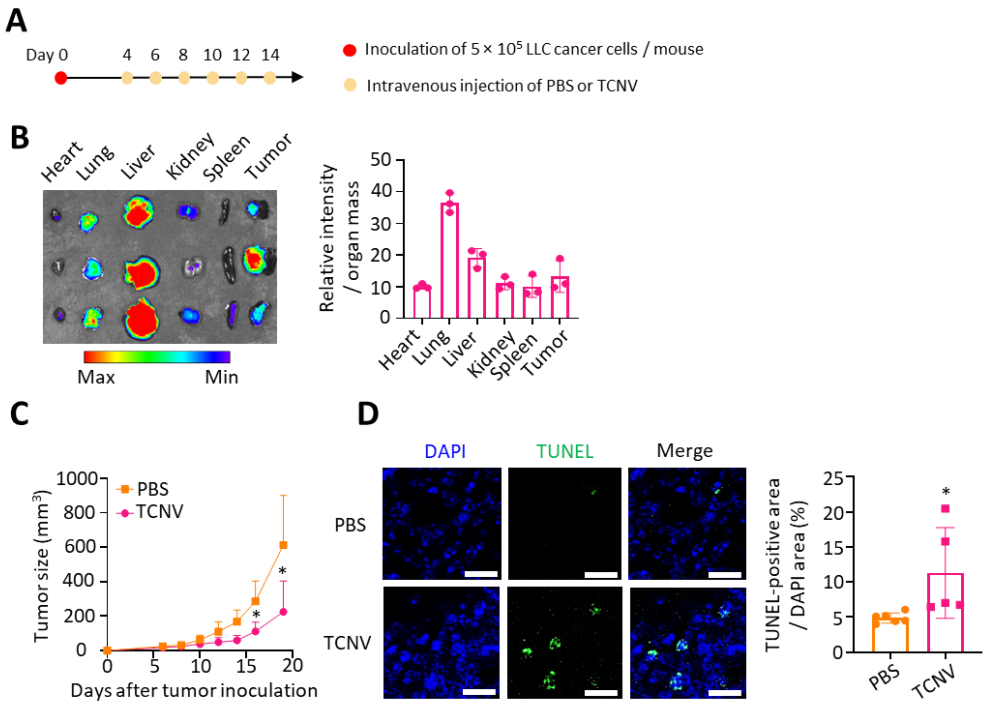

Figure 2.8 Biodistribution and antitumor efficacy of intravenously injected TCNVs.

A) Experimental scheme of intravenous injection of TCNVs. **B)** Biodistribution of intravenously injected TCNVs in major organs and tumor. Relative intensity / organ mass was calculated. **C)** Tumor growth profile of LLC tumor model. **D)** TUNEL assay of tumor tissues. Statistic significance was calculated by Student's t-test or two-way ANOVA with Bonferroni post-tests. * $p < 0.05$ versus PBS.

2.2.8. In vivo toxicity of TCNVs

In addition, intravenous injection of TCNVs showed no notable toxicity in vivo, as evaluated by serum analysis (Figure 2.9A, 2.9B) and histological analysis of the major organs (Figure 2.9C).

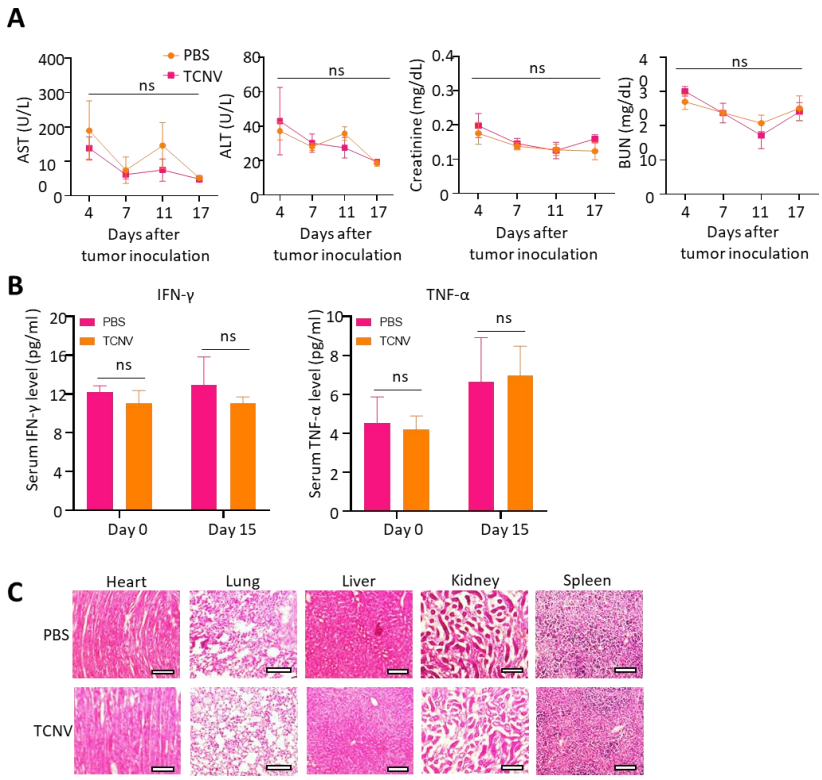

Figure 2.9 In vivo toxicity of intravenously injected TCNVs.

A) Serum level of AST, ALT, Creatinine, and BUN. n = 5. **B)** Serum level of pro-inflammatory cytokines, IFN- and TNF- in TCNV treated mice at day 0 and day 15. Day 15 is 24 hrs after last injection. n = 3. **C)** H&E staining of major organs in TCNV treated mice at day 21. Scale bar = 100 μm. ns = not significant. Statistical significance was calculated by multiple t-tests with Holm-Sidak correction or two-way ANOVA with Bonferroni post-tests.

2.2.9. In vitro exhaustion test of TCNVs

While T cell therapy is susceptible to harsh immune suppression in TME,[21] TCNVs can reverse the immunosuppressive TME whilst maintaining their anti-tumoral efficacy. To determine whether TCNVs can resist the immune suppression, I treated T cells and TCNVs with recombinant PD-L1 proteins in vitro. The PD-L1 treatment induced exhaustion of OT-1 $CD8^+$ T cells, as demonstrated by significant reduction in cancer cell lysis at various effector-to-target (E:T) ratios (Figure 2.10A). aPD-L1 treatment to PD-L1-treated T cells inhibited the T cell exhaustion, as indicated by increase in the cell lysis rate by aPD-L1. Importantly, TCNVs maintained their anti-tumoral activity upon PD-L1 treatment. Moreover, in contrast to T cells exhausted by TGF-β treatment, the anti-tumoral activity of TCNVs was not affected by TGF-β treatment (Figure 2.10B). Altogether, these data showed that TCNVs, unlike T cells, do not suffer from the tumor's immunosuppressive mechanisms and can maintain their anti-tumoral efficacy in the immunosuppressive TME, emphasizing their advantage over T cell therapy.

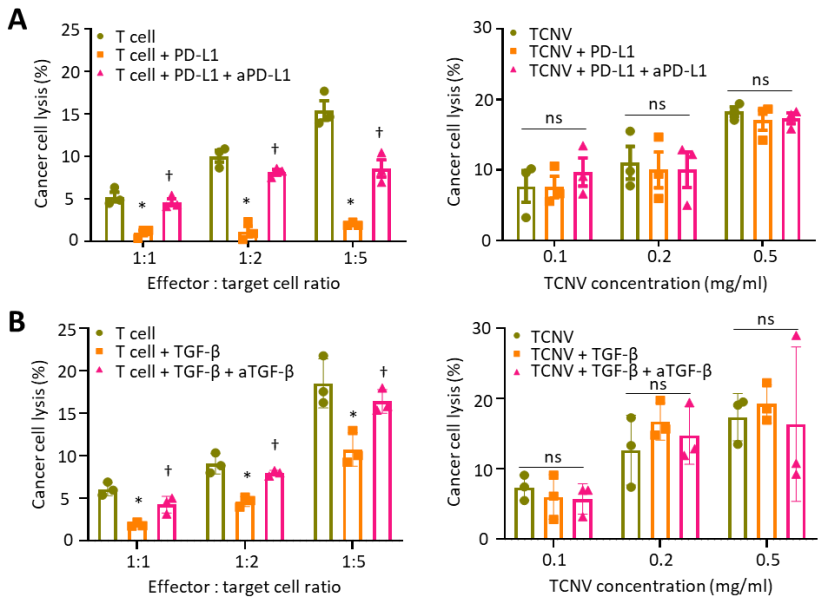

Figure 2.10 In vitro exhaustion test of TCNVs.

In vitro lysis of E.G7-OVA cancer cells by OT-1 CD8+ T cells or TCNVs. In vitro immune suppression was induced by recombinant PD-L1 **(A)** or recombinant TGF-β **(B)**. The addition of aPD-L1 or aTGF-β rescued

T cells from exhaustion. n = 3. ns = not significant. Statistical significance was calculated by one-way ANOVA with Tukey's significant difference multiple comparisons. * $p < 0.05$ versus T cell; † $p < 0.05$ versus T cell + PD-L1 in (A); versus T cell + TGF-β in (B).

2.2.10. In vivo exhaustion test of TCNVs

Lastly, tumor suppression abilities of T cells and TCNVs with the exhaustion signal PD-L1 were compared in vivo (Figure 5C and 5D). Recombinant PD-L1 proteins together with either OT-1 $CD8^+$ T cells or TCNVs were injected to E.G7-OVA tumor-bearing mice. The injection of either OT-1 $CD8^+$ T cells or TCNVs significantly suppressed the tumor growth. The PD-L1 treatment significantly reduced the in vivo anti-tumoral activity of OT-1 $CD8^+$ T cells (Figure 5C). TIL analysis revealed that $CD8^+$ T cells in tumors in the T cell + PD-L1 injection group expressed higher levels of PD-1, a marker of $CD8^+$ T cell exhaustion,[39] indicating that PD-L1 induced $CD8^+$ T cell exhaustion in tumors. In contrast, TCNVs showed a resistance to PD-L1-mediated exhaustion and a persistent tumor-killing ability (Figure 5D). PD-L1 injection did not affect PD-1 expression on tumor infiltrating $CD8^+$ T cells. In addition, immunohistochemistry of the tumor tissues for cleaved caspase-3, which represents granzyme B-mediated cytotoxic function of $CD8^+$ T cells or TCNVs, suggested that PD-L1 reduced the cytotoxicity of $CD8^+$ T cells (Figure 5E). In contrast, PD-L1 did not affect the cytotoxicity of TCNVs (Figure 5F), indicating that TCNVs do not undergo PD-L1-mediated exhaustion.

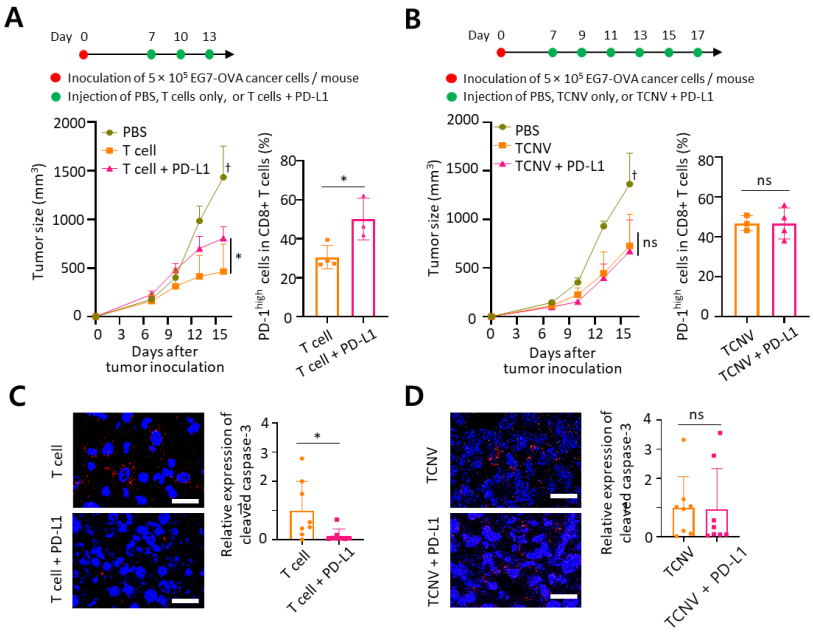

Figure 2.11 In vivo exhaustion test of TCNVs.

In vivo E.G7-OVA tumor growth following intratumoral injection of OT-1 CD8+ T cells **(A)** or TCNVs **(B)** with or without exogenous PD-L1 to tumor-bearing mice. n = 5. Exhaustion of CD8+ T cells was evaluated by determining percentage of PD-1^{high} cells in CD8+ T cells in the tumor tissues at day 17. n = 3–4. **C, D)** Immunohistochemistry staining for cleaved caspase-3 (red) in E.G7-OVA tumor sections at day 17. Blue is DAPI. Scale bars: 100 μm. n = 7–8. ns = not significant. Statistical significance was calculated by Student's t-tests or two-way ANOVA with Bonferroni post-tests. * $p < 0.05$ versus T cell; † $p < 0.05$ PBS versus T cell, T cell + PD-L1, TCNV, or TCNV + PD-L1 in (A) and (B).

2.2.11. Discussion

Here I developed TCNV, a T-cell-derived anti-cancer agent for cancer immunotherapy. TCNVs suppressed tumor in two mechanisms, reversing immunosuppressive TME and directly killing cancer cells. As the immunosuppressive TME is one of the major hurdles in adoptive T cell therapy for solid tumors, there have been continuous attempts to reverse the TME. Immune checkpoint blockades, including anti-PD-1 antibody and anti-PD-L1 antibody, can inhibit T cell exhaustion in the immunosuppressive TME and have shown remarkable clinical outcomes in solid tumor treatment[40-44]. TCNV may be superior to the current immune checkpoint blockades due to the following features. TCNV can reverse the immunosuppressive TME not only by inhibiting PD-1/PD-L1 interaction but also by scavenging TGF-β. Furthermore, TCNV can directly induce tumor cell apoptosis via granzyme B delivery. Unlike cytotoxic T cells, the anti-tumoral activity of TCNV is not affected by interactions with immunosuppressive molecules in the immunosuppressive TME. Thus, TCNV can maintain its anti-tumoral activity in the immunosuppressive TME of solid tumors (Figure 5). However, there are some limitations of TCNVs to address. First, while 10% of TCNVs can reach to tumor tissues, rest of the nanovesicles may cause unexpected toxicity due to granzyme B delivery. To circumvent this problem, may be further targeting moiety is needed to TCNVs, such as antibody conjugation or targeting peptides.

Moreover, efficient ex vivo expansion of $CD8^+$ T cells is required for clinical application. In the present study, I produced TCNVs from $CD8^+$ T cells isolated from OT-1 transgenic mice because of facile ex vivo expansion of OT-1 $CD8^+$ T cells using ovalbumin peptides and IL-2. Dynabead® or another novel T cell expansion platform[45] could be used for ex vivo expansion of autologous $CD8^+$ T cells isolated from patients. Although OT-1 $CD8^+$ T cells are different from polyclonal human T cells in TCR diversity, the TCR does not affect the anti-tumor mechanisms or efficacy of TCNVs. Taken together, the TCNV therapy may be an effective cancer-immunotherapy that resists immunosuppression mechanisms of solid tumors.

2.3. Experimental section

2.3.1. Preparation of TCNVs

TCNVs were prepared from activated OVA-specific $CD8^+$ T cells from OT-1 transgenic mice (OT-1 $CD8^+$ T cells). OT-1 $CD8^+$ T cells have an MHC class I- restricted OVA-specific TCR that recognizes the SIINFEKL peptide ($OVA_{257-264}$) of ovalbumin. Spleens and peripheral lymph nodes were harvested from OT-1 TCR transgenic mice, a generous gift from Professor Chang-Yuil Kang in Seoul National University, and were dissociated to obtain a single-cell suspension. Red blood cells were lysed using ACK lysis buffer (Gibco, NY, USA). The single cells were resuspended in RPMI 1640 (Gibco) containing 10% (v/v) fetal bovine serum (FBS, Gibco) and 1% (v/v) penicillin/streptomycin (PS, Gibco), 0.05 mM β-mercaptoethanol (Sigma Aldrich, MO, USA), and 1 mg/ml $OVA_{257-264}$ (ANASPEC, CA, USA). After 48 hrs, an aliquot of the cells was cultured in RPMI 1640 supplemented with murine IL-2 (5 ng/ml, Biolegend, CA, USA) for 2 days. Activated OVA-specific-CD8+ T cells were isolated using Histopaque®-1077 (Sigma Aldrich). The cells were then collected and serially extruded through polycarbonate membrane filters (Whatman, UK) with pore sizes of 1 μm, 400nm and 200 nm using a mini-extruder (Avanti Polar Lipids, AL, USA) to obtain NVs as previously reported.[12,46] The NVs were then ultracentrifuged in a density gradient formed by 10 and 50% OptiPrep layers

(Sigma Aldrich) at 100,000 g for 2 hrs at 4 °C. The vesicles obtained from the interface of the layers were further ultracentrifuged at 100,000 g for 2 hrs at 4 °C. The protein concentration of the isolated TCNVs was quantified using Bradford reagent (Sigma Aldrich) according to the manufacturer's protocol. To produce trTCNVs, TCNVs were treated with 2.14 mM trypsin for 1 hr.

2.3.2. Characterization of TCNVs

The size distributions and zeta potential of TCNVs were assessed by dynamic light scattering and electrophoretic light scattering (Zetasizer Nano ZS, Malvern Panalytical, UK), respectively. The morphology of TCNVs was evaluated with a JEM-2100 transmission electron microscope (JEOL, Japan) after TCNVs were stained with 1% (v/v) uranyl acetate. Flow cytometric analysis was performed after reaction with antibodies against granzyme B and PD-1 to identify proteins on trTCNVs, TCNVs, and activated OT-1 $CD8^+$ T cells. trTCNVs or TCNVs were adsorbed onto 4 μm aldehyde/sulfate latex beads (Invitrogen, CA, USA), respectively, and then trTCNVs or TCNVs-bound beads were stained with anti-PD-1 antibodies (Biolegend) or anti-granzyme B antibodies (Biolegend). For granzyme B detection, eBioscience™ Intracellular Fixation & Permeabilization buffer set (Invitrogen) was used for intracellular staining. After washing, the stained specimens were analyzed with Becton Dickinson FACS Canto-II flow cytometer (BD Biosciences, CA, USA).

2.3.3. Cell Culture

LLC lung cancer cells were purchased from American Type Culture Collection (ATCC, VA, USA). E.G7-OVA cells, a variant of EL4 cell line that expresses full-length OVA, was a gift from Professor Junsang Doh, Seoul National University, Seoul, Korea. LLC cells were cultured in Dulbecco's Modified Eagle's Medium (DMEM) (Gibco, NY, USA) supplemented with 10% (v/v) FBS and 1% (v/v) PS. E.G7-OVA cells were cultured in RPMI 1640 containing 10% (v/v) FBS, 1% (v/v) PS, 10 mM HEPES, 1.0 mM sodium pyruvate, 0.05 mM β-mercaptoethanol and 0.04 μg/ml G-418 antibiotics (Roche). Primary T cells were isolated from spleens of 6-week-old female C57BL/6 mice (Orient Bio, Gyeonggi, Korea) using MojoSort™ Mouse CD8 T Cell Isolation Kit (Biolegend) according to the manufacturer's protocol. The cells were then cultured in RPMI 1640 supplemented with 10% (v/v) FBS, 1% (v/v) PS, 1% (v/v) GlutaMAX (Gibco), 10 mM HEPES, 1 mM sodium pyruvate, and 55 μM 2-mercaptoethanol.

2.3.4. PD-L1- mediated nanovesicles binding to cancer cells

LLC cancer cells were seeded in 6-well confocal plates at 5×10^5 cells per well prior to TCNV treatment. trTCNVs and TCNVs were stained with DiI (1,1'-Dioctadecyl-3,3,3',3'-Tetramethylindocarbocyanine Perchlorate, Invitrogen) for 2 hrs and washed with PBS twice. The cytoplasm of LLC cancer cells were stained with DiO(3,3'-Dioctadecyloxacarbocyanine Perchlorate, Invitrogen) for 2 hrs and washed with PBS twice. DiI-stained trTCNVs or TCNVs were treated to cancer cells for 1 hr and washed thrice. For the PD-L1 antibody (aPD-L1, Biolegend) treatment group, the antibodies were added to the culture at 0.5 μg/ml concentration. The cells were fixed with 4 % PFA (Biosesang, Korea). The cell nuclei were stained with DAPI (Vector Laboratories, CA) for 10 min. Confocal microscopic images were obtained and the mean intensity of red fluorescence was calculated. Calculated data were analyzed using NIH ImageJ software (Bethesda, MD, USA).

2.3.5. Prevention of T cell exhaustion by TCNVs

E.G7-OVA cells were seeded in 96-well plates at 4×10^4 cells per well. Prior to co-culture, T cells were treated with 0.5 μg/ml recombinant mouse PD-L1 protein (Biolegend) for 30 min to induce T cell exhaustion in vitro. For the PD-L1 antibody-treated group, 0.5 μg/ml antibodies were added to E.G7-OVA cell cultures. For the PbTCNV and TCNV groups, 0.05 mg/ml of nanovesicles were added to E.G7-OVA cell cultures for PD-L1 blocking and incubated for 30 min. Then T cells were cocultured with the E.G7-OVA cells for 4 hrs, then LDH release assay (DoGenBio, Seoul, Korea) was performed according to manufacturer′s protocol. To exclude direct killing of tumor cells by TCNVs, the levels of LDH released from E.G7-OVA cells treated with 0.05mg/ml of PbTCNVs or TCNVs without T cell cocultures were subtracted from the levels of PbTCNV and TCNV groups. For TGF-β-mediated exhaustion prevention tests, E.G7-OVA cells were treated with 0.42 μg/ml of recombinant TGF-β protein (Biolegend) and the same amount of antibodies or nanovesicles were added as the PD-L1 prevention tests. After 4 hrs of coculture, the LDH release assay was performed to evaluate T cell-mediated tumor killing capacity after TGF-β treatment.

2.3.6. TCNV uptake by cancer cells

LLC cancer cells (5×10^5 cells) were seeded in 6-well confocal plates. Prior to TCNV treatment, cancer cells were stained with Lysotracker Red (Invitrogen) for 1 hr for lysosome staining. trTCNVs and TCNVs were stained with DiD (1,1'-Dioctadecyl-3,3,3',3'-Tetramethylindodicarbocyanine, Invitrogen) for visualization. Then, cancer cells were washed with PBS thrice. The cells were treated with trTCNVs or TCNVs for 4 hrs and washed thrice. The cells were fixed with 4 % PFA and washed with PBS for 3 times. The cell nuclei was stained with DAPI for 10 min. Fluorescence images of the cell were obtained by LSM 710 (Carl Zeiss, Germany) installed at the National Center for Inter-university Research Facilities (NCIRF) at Seoul National University.

2.3.7. Granzyme B delivery by TCNVs to cancer cells

LLC cancer cells (5×10^5 cells) were seeded in 6-well confocal plates. Prior to TCNV treatment, the cytoplasm of cancer cells was stained with DiI for 2 hrs. The cancer cells were washed with PBS thrice and treated with trTCNVs or TCNVs for 4 hrs. Then, the cells were washed thrice, fixed with 4 % PFA and permeabilized with 0.6 % Triton X-100 (Sigma Aldrich) and 10% Horse serum (Gibco) in PBS for 45 min. The cells were incubated with anti-granzyme B antibodies (Biolegend) overnight in 4 ℃. The unbound antibodies were washed with PBS for 3 times and the cell nuclei was stained with DAPI for 10 min. Fluorescence images of cell were obtained by LSM 710 (Carl Zeiss, Germany).

2.3.8. TCNV cytotoxicity on tumor cells

LLC cancer cells (5×10^4 cells) were plated in 24-well plates a day before nanovesicle treatment. trTCNVs or TCNVs were treated at 0.2 mg/ml concentration per well (n = 3). For a control group, the same volume of PBS was added. After 24 hrs, the cancer cells were detached with trypsin-EDTA and lysed for western blot analysis or stained with Annexin V/PI kits (Biolegend). For PCR analysis, 5×10^5 LLC cancer cells were plated in 6-well plates a day prior nanovesicle treatment. Then, trTCNVs or TCNVs were treated at 0.2 mg/ml concentration per well (n = 3). After 4 hrs, the cancer cells were washed with PBS. mRNA were extracted by QIAzol Lysis Reagent (Qiagen, CA, USA). RNAs from each group were used for cDNA synthesis using PCR PreMix (Bioneer, Daejeon, Korea). SYBR green-based qRT-PCR was performed with TOPreal™ qPCR 2X PreMIX (Enzynomics, Daejeon, Korea). The cycling conditions were as follows: initial denaturation at 95 ℃ for 15 min, followed by 60 cycles at 95 ℃ for 10 s, 60 ℃ for 15 s, and 72 ℃ for 30 s. Each gene expression was normalized by GAPDH expression. For cleaved caspase-3 staining, TCNV-treated LLC cancer cells were fixed with 4 % PFA and permeabilized with 0.6 % Triton X-100 and 10% Horse serum in PBS for 45 min. Then, the cells were incubated with anti-mouse cleaved caspase 3 antibodies (Cell Signaling Technology, MA, USA) overnight, 4 ℃. The unbound antibodies were removed, and the cell nuclei were stained with DAPI for 10 min.

Fluorescence images were obtained by LSM 710 (Carl Zeiss). For flow cytometry analysis, the cells were stained with APC-Annexin V and PI according to the manufacturers' protocol. Fluorescently stained cells were analyzed with BD Canto-II flow cytometer (BD Sciences). The percentage of Annexin V/PI double positive cells was calculated as apoptotic cells.

2.3.9. Mice

Six-week-old female C57BL/6 mice were purchased from Orient Bio. All the animal experiments were approved by the Institutional Animal Care and Use Committee (IACUC) of Seoul National University (SNU-190306-03-1) and performed in compliance with the guidelines of the IACUC.

2.3.10. In vivo tumor growth

C57BL/6 mice were anesthetized with rumpun (10 mg/kg) and ketamine (100 mg/kg), and injected with LLC cancer cells (5×10^5 cells in 100 μL PBS per mouse) subcutaneously on the right flank. After 7 days, the tumor-bearing mice were randomly divided into three groups and intratumorally injected with either PBS, trTCNVs or TCNVs (100μg nanovesicles in 50 μl PBS). The tumor sizes were measured every 2 days using a digital caliper and computed according to the ellipsoidal calculation: $V = 0.5 \times (\text{longest diameter}) \times (\text{shortest diameter})^2$. The survival of the mice was monitored for 55 days. The mice bearing tumor exceeding 2500 mm^3 size were euthanized with CO_2 inhalation. For intravenous injection of TCNVs to tumor-bearing mice, LLC cancer cells were injected subcutaneously in the same manner. After 4 days, PBS or TCNVs (300μg nanovesicles in 100μl PBS) were intravenously injected. The tumor sizes were measured every 2 days. For immunohistochemistry staining of tumor tissues, tumor tissues were obtained from mice 4 days after last injection.

2.3.11. Tumor infiltrating lymphocyte analysis

Tumor infiltrating lymphocytes were analyzed as previously described[37]. Briefly, 4 days after last injection, tumor masses were harvested from euthanized mice, and the tumor masses were weighed. Then, the tumor tissues were minced and passed through a 70-μm sized pore filter. Separated single cells were stained with following antibodies: anti-mouse CD3, anti-mouse CD4, anti-mouse CD8, anti-mouse Foxp3, anti-mouse IFN-γ, anti-mouse TNF-α, and anti-mouse granzyme B (Biolegend). Intracellular staining of tumor infiltrating lymphocytes were conducted according to the manufacturer's protocol. The staining results were analyzed using FlowJo software (Tree Star Inc., OR, USA).

2.3.12. Immunohistochemistry staining of tumor sections

Tumor tissues were fixed in 4% PFA and kept in 30 % sucrose solution for a day. The fixed tissues were embedded in OCT (Scigen scientific, CA, USA) and stored in – 80 ℃. The cryopreserved tissues were sectioned at 10 μm thickness using a cryostat microtome (Leica, Germany). For cleaved caspase-3 staining, tissue sections were washed with PBS twice, blocked and permeabilized with 0.6 % Triton X-100 and 10 % donkey serum (Gibco) in PBS for 2 hrs. Then, the sections were incubated with anti-mouse cleaved caspase 3 antibodies (Cell Signaling Technology) overnight, 4 ℃. The unbound antibodies were removed and the cell nuclei was stained with DAPI for 10 min. Fluorescence images were obtained by LSM 710 (Carl Zeiss). For terminal deoxynucleotidyl transferase-mediated dUTP nick end labeling (TUNEL) assays, tumor tissue sections were washed and stained with DeadEnd™ Fluorometric TUNEL System (Promega, WI, USA) according to the manufacturer's protocol. Images were obtained by LSM 710 (Carl Zeiss), and TUNEL-positive cell percentages were calculated using NIH ImageJ software (Bethesda).

2.3.13. TCNV biodistribution

Mice were anesthetized with an injection of rumpun (10mg/kg) and ketamine (100 mg/kg). LLC cancer cells (1×10^6 cells per mouse) were injected into the right flanks of 6-week-old C57BL/6 mice to develop subcutaneous tumors. TCNVs were stained with VivoTrack 680 (Perkin Elmer, MA, USA) according to the manufacturer's protocol. TCNVs (300 μg) were suspended in 100 μl PBS and intravenously injected into the mice via the tail vein (n = 4 animals). To monitor the distribution of intravenously injected TCNVs, the mice were sacrificed 24 hrs after the injection. The major organs (heart, lung, liver, kidney, and spleen) and tumors were retrieved. Fluorescence signals were acquired using IVIS spectrum computed tomography (Perkin Elmer) at 680 nm excitation and quantified in using Living Image 3.1 software. The fluorescence intensity of each organ or tumor was normalized to the sum of intensities of the organs and tumors in each group.

2.3.14. In vivo toxicity of TCNVs

C57BL/6 mice were anesthetized with rumpun (10 mg/kg) and ketamine (100 mg/kg), and injected with LLC cancer cells (5×10^5 cells in 100 μL PBS per mouse) subcutaneously on the right flank. After 7 days, the tumor-bearing mice were randomly divided into three groups (PBS, trTCNVs and TCNVs) and intratumorally injected with 100μg nanovesicles in 50μl PBS. Blood sample was obtained at various time points. Serum was obtained from the blood by centrifugation at 3000 g for 10 min. The levels of AST, ALT, creatinine and BUN in the serum were determined by DRI-CHEM 3500S chemistry analyzer (Fujifilm, Japan). For histological analysis, major organs (liver, lung, spleen, heart, and kidney) were retrieved 26 days after tumor modeling. The tissues were fixed with 4% PFA overnight at 4 °C, and dehydrated in 30% sucrose solution. The tissues were embedded in OCT compound (Scigen scientific) and sectioned to a thickness of 10 μm using a cryostat microtome (Leica, Germany). The sections were stained with hematoxylin (Cancer Diagnostics, NC, USA) and eosin (BBC Biochemical, WA, USA), and imaged using an optical microscope (Olympus, Tokyo, Japan). In tumor-bearing mice with intravenous injection of TCNVs, blood samples were obtained at day 4, 7, 11, and 17 and analyzed. Major organs were harvested at day 17 and stained with hematoxylin and eosin for toxicity diagnosis.

2.3.15. In vitro exhaustion of T cells and TCNVs

E.G7-OVA cells were seeded in 96-well plates at 4×10^4 cells per well. Prior to co-culture, T cells were treated with 0.5 μg/ml recombinant mouse PD-L1 protein (Biolegend) for 30 min to induce T cell exhaustion in vitro. In the anti-PD-L1 antibody-treated groups, 0.5 μg/ml antibodies were added. T cells were washed twice with PBS and co-cultured with the tumor cells at various effector-to-target (E:T) ratios (1:1, 1:2 and 1:5). In the TCNV-treated groups, PD-L1 protein and aPD-L1 were treated in the same manner. TCNVs were treated to cancer cells at various doses, 10μg, 20μg and 50μg per well. After 4 hrs, LDH release assay was used according to the manufacturer's protocol. The same analysis was performed with TGF-β protein to investigate TGF-β mediated exhaustion in T cells and TCNVs in vitro.

2.3.16. In vivo exhaustion of $CD8^+$ T cells and TCNVs

C57BL/6 mice were anesthetized and injected with E.G7-OVA cancer cells (5×10^5 cells in 100 μL PBS per mouse) subcutaneously on the right flank. After 7 days, the tumor- bearing mice were randomly divided into five groups (PBS, OT-1 $CD8^+$ T cells, OT-1 $CD8^+$ T cells + PD-L1 protein, TCNVs and TCNVs + PD-L1 protein) and intratumorally injected with 1×10^6 OT-1 $CD8^+$ T cells or 100 μg nanovesicles in 50μl PBS. PD-L1 proteins were injected intratumorally at every injection time points. The tumor sizes were measured every 3 days. Four days after last injection, the mice were euthanized and tumor masses were harvested. For tumor infiltrating lymphocytes analysis, lymphocytes were separated from the tumor tissues and stained with anti-CD3 antibody, anti-CD8 antibody, and anti-PD-1 antibody (Biolegend) for determination of exhausted T cell population.

2.3.17. Statistical analysis

Unless stated otherwise, data were presented as mean ± standard deviation (SD). The data were analyzed by one-way analysis of variance (ANOVA) with Turkey's significant difference multiple comparisons to calculate P values for comparisons between more than two groups. Two-way ANOVA with Bonferroni's correction was used to calculate P values for comparisons between groups over multiple time points. The log-rank test was used to compare survival differences for Kaplan–Meier plots using Prism software (GraphPad, CA, USA).

Chapter 3. Senescent cancer cell-derived nanovesicle as a personalized therapeutic cancer vaccine

3.1. Introduction

Therapeutic cancer vaccines (TCVs), another cancer immunotherapy approach, involve the administration of immunogenic tumor antigens to stimulate patients' adaptive immune system against tumors.[47] The basic principles of TCV include delivery of tumor antigens to dendritic cells (DCs), DC activation, DC migration to secondary lymphoid organs, and activation of tumor-reactive T cells that are responsible for killing cancer cells. However, the development of clinically applicable TCVs has been limited thus far. A tumor antigen-loaded DC-based TCV (Sipuleucel-T) was approved by the FDA in 2010 to treat prostate cancer.[48] Since then, no TCV has been approved. Difficulty in the identification of immunogenic tumor antigens and insufficient antitumor immunity of TCVs are the main limitations in the development of clinically applicable TCVs.[49]

A key step in the TCV development process is the identification of immunogenic tumor antigens that elicit antitumor immunity. Various tumor-associated antigens (TAAs), which are highly expressed in cancer cells, have been suggested as new target antigens for TCV. TAAs include human epidermal growth factor receptor-2 (HER-2), mesothelin and melanoma-associated antigen recognized by T cells (MART-1).[50,51] Recently,

neoantigens, which are nonself antigens that are absent from normal cells and expressed only in mutated cancer cells, have emerged as new target antigens for TCV. Neoantigens can be profiled by next-generation sequencing-based cancer exome sequencing.[8,52] However, most TCVs employing TAAs or neoantigens have failed to show therapeutic benefit in clinical trials.[53,54]

The disappointing clinical results of TCVs employing TAAs is mainly due to the non-exclusive and heterogeneous expression of TAAs in tumor tissues.[8] For effective cancer vaccination, T cells activated by TCVs should recognize tumor antigens on cancer cells. However, TAAs are also expressed in normal tissues, resulting in off-target side effects of activated T cells or elimination of TAA-specific T cells through immune tolerance. In addition, heterogeneous expression of TAAs in tumor leads to low effectiveness in vaccine-mediated killing of tumors.

Meanwhile, neoantigens are highly individual-specific and only a small number of neoantigens are shared between cancer patients.[8] This demands the development of personalized TCVs. Recently, next-generation sequencing technology and whole genome mapping have made it feasible to identify patient-specific neoantigens and have promoted the design of personalized TCVs.[55] However, most of discovered neoantigens exhibit low immunogenicity or low affinity for major histocompatibility complex (MHC). Profiling of cancer patients revealed that only a small fraction (~1-2%) of neoantigens in cancer cells are recognized by T cells and induce

sufficient immune responses.[56] In addition, some neoantigens often disappear in tumor tissues due to rapid mutations in tumor cells. This poses a problem regarding current approach of personalized TCV development that involves identification of patient-specific neoantigens and subsequent selection of target neoantigens.

Nanovaccines made of autologous cancer cell membrane have been proposed as personalized TCVs that do not require identification of immunogenic tumor antigens.[57,58] Inducing effective antitumor immune responses is a critical issue for effective TCV. Induction of sufficient antitumor immune responses in vivo may not be achieved by tumor antigens alone and often requires the use of an appropriate exogenous adjuvant that provokes DC activation.[59] Several adjuvants that stimulate DC Toll-like receptor (TLRs) have been used to improve the immunogenicity of TCVs. Nanovaccines made of autologous cancer cell membrane generally require exogenous adjuvants (e.g., TLR agonists) to improve the vaccine immunogenicity. These adjuvants include CpG oligodeoxynucleotides (CpG ODNs), resiquimod (R848), and polyinosinic:polycytidylic acid (poly I:C).[60,61] However, these TLR agonists raise safety concerns.[62,63] The use of safe and effective adjuvants is required for safe and effective TCV therapy.

Here, I present senescence-induced cancer cell-derived nanovesicle (SCCNV) as a personalized TCV that can overcome the limitations of current TCVs. Nanovesicles are exosome-mimetic nano-sized vesicles produced by extruding cells through nano-porous membranes. Nanovesicles

can deliver RNAs and proteins originated from parental cells and showed higher production efficiency than naturally secreted exosomes.[12] Nanovesicles derived from various immune cells, including T cell, macrophage and dendritic cell, have been explored for cancer immunotherapy.[64-66] SCCNVs were produced by serial extrusion of senescence-induced cancer cells (Figure 3.1A). Autologous cancer cells for SCCNV preparation would be clinically available from the blood of liquid cancer patients or from tumors removed surgically from solid cancer patients. SCCNVs prepared from autologous cancer cells can deliver a variety of patient-specific tumor antigens, avoiding complicated process of neoantigen identification. While TCVs with a single TAA or neoantigen may face immune escape that is caused by ceaseless mutations of cancer cells in vivo and subsequent disappearance of TAA or neoantigen, SCCNVs that would contain a spectrum of tumor antigens may avoid the immune escape problem. Cellular senescence is a phenomenon characterized by arrest in cell division in response to various cellular stresses, such as DNA damage, oxidative stress, and oncogenic activation.[67] Senescent cells express senescence-associated secretory phenotypes (SASPs), including IFN-γ and TNF-α.[68] In the present study, IFN-γ and TNF-α were expressed during ex vivo senescence induction of cancer cells and contained in SCCNVs. These endogenous cytokines served as adjuvants that enhance the immunogenicity of the vaccine. These endogenous adjuvants would be safer than conventional exogenous adjuvants such as MPLA, poly I:C and CpG

that raise safety concerns.[62,63] Intradermally injected SCCNVs can deliver tumor antigens and adjuvants (IFN-γ and TNF-α) to DCs, resulting in DC activation, DC migration to draining lymph nodes, and activation of tumor-specific T cells that are responsible for cancer cell killing (Figure 3.1B).

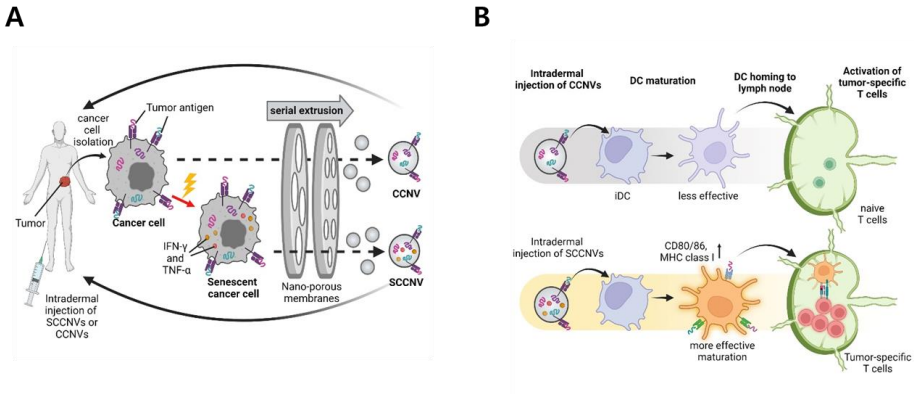

Figure 3.1 Experimental design of SCCNVs.

Illustration of **A)** SCCNV preparation and personalized cancer vaccination and **B)** proposed mode of action of the vaccines. SCCNV = senescent cancer cell nanovesicle. CCNV = cancer cell nanovesicle. iDC = immature dendritic cell. mDC = mature dendritic cell. Created from Biorender.com.

3.2. Results and Discussion

3.2.1. Characterization of SCCNVs

To induce senescence in B16F10 melanoma cells, the cells were treated with various concentrations of doxorubicin. Senescence-associated beta-galactosidase (SA-β-gal) staining showed that doxorubicin concentrations higher than 0.1 μM successfully induced senescence. Doxorubicin concentration of 0.1 μM resulted in the highest cell viability (Figure 3.2A, 3.2B). Thus, I chose 0.1 μM as the optimal concentration of doxorubicin and used this concentration in the following experiments, which is 100 times lower than that used in clinical chemotherapy. Furthermore, the residual doxorubicin after doxorubicin treatment on cells was removed prior to use of SCCNVs in experiments, so doxorubicin itself would not exert antitumor effects in SCCNV therapy. The mRNA expression levels of p16 and p21, cellular senescence markers, increased in B16F10 cells treated with 0.1 μM doxorubicin (Figure 3.2C). In addition, the mRNA and protein levels of IFN-γ and TNF-α, both of which are SASPs induced in senescent cells, increased in B16F10 cells treated with 0.1 μM doxorubicin (Figure 3.2D, 3.2E). Transmission electron microscopy (TEM) analysis showed a unilamellar structure with lipid bilayers of SCCNVs (Figure 3.3A). SCCNVs showed hydrodynamic diameters of 226.1 ± 24.6 nm, as revealed by dynamic light scattering analysis (Figure 3.3B), and zeta potential of SCCNVs was -20.2 ± 8.7 (Figure 3.3C). Hydrodynamic

diameter of SCCNVs were investigated for a week, and the result showed the size of SCCNVs were stably maintained in serum-containing buffer for at least 7 days (Fig. 3.3D). Increased IFN-γ and TNF-α levels in senescence-induced cells were preserved in SCCNVs at both mRNA and protein levels (Figure 3.3E, 3.3F). The amount of INF- γ and TNF- α in SCCNVs were quantified by Enzyme-linked immunosorbent assay (ELISA), and approximately 4.56 pg of IFN-γ and 0.14 pg of TNF-α were included in 1 ug of SCCNVs (Figure 3.3G). Lastly, coomassie blue staining revealed that senescence induction did not change protein profiles in B16F10 cancer cells, and SCCNVs preserved most of the proteins from senescent B16F10 cancer cells, with a small variation possibly due to a relative increase in cell surface proteins through nanovesicle production (Figure 3.3H).[12]

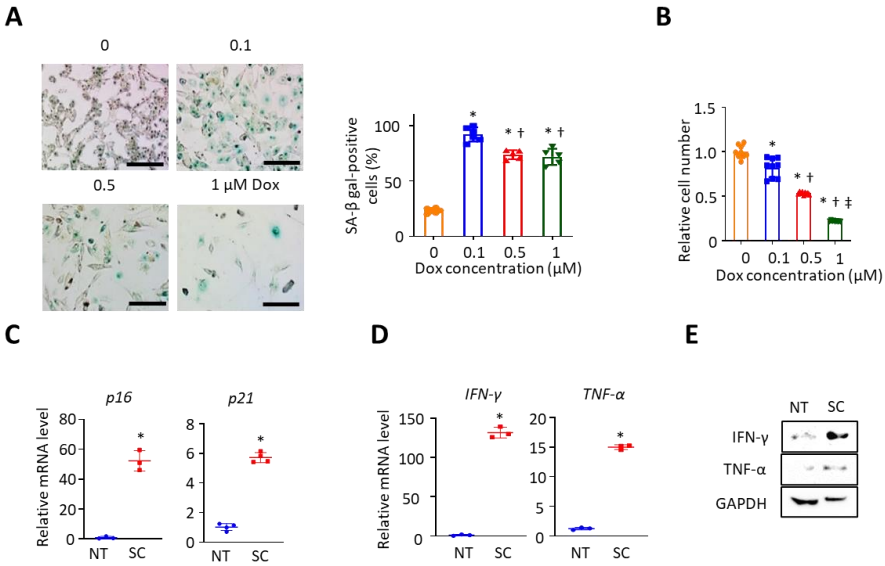

Figure 3.2 Optimization of senescence induction in B16F10 cancer cells. **A)** SA β-gal staining (green) of B16F10 cancer cells following senescence induction with treatment with various concentrations of doxorubicin for 4 days. Scale bars = 100 μm. **B)** Optimization of Dox concentration: cell number relative to initial cell number after doxorubicin treatment at various concentrations for 4 days. **C)** mRNA levels of e) p16, p21**, D)** IFN-γ and TNF-α, and **E)** protein levels of IFN-γ and TNF-α in B16F10 cancer cells after senescence induction with 0.1 μM doxorubicin. NT = no treatment. SC = senescence induction. Data represent mean ± SD. Statistical significance was calculated by Student's t-tests (e, f, and k) or one-way analysis of variance (ANOVA) with Tukey's significant difference multiple comparisons (a, b, and m).* $P < 0.05$ versus NT or 0 μM doxorubicin in (a)-(f); versus CCNV in (i). † $P < 0.05$ versus 0.1 μM in (a) and (b), ‡ $P < 0.05$ versus 0.5 μM in (b).

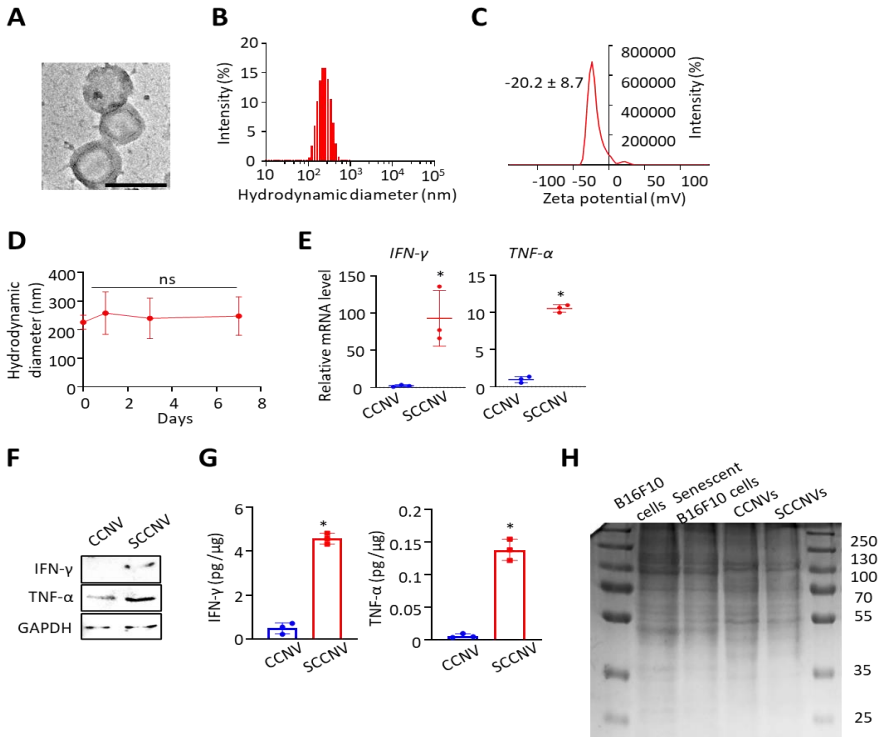

Figure 3.3 Characterization of SCCNVs.

A) Transmission electron microscopic image of SCCNVs. Scale bar = 250 nm. **B)** Hydrodynamic diameter of SCCNVs. **C)** Zeta potential analysis of SCCNVs. **D)** Hydrodynamic diameter of SCCNVs incubated in 10 % (v/v) serum-containing buffer for various time periods, showing colloidal stability of SCCNVs. Relative **E)** mRNA and **F)** protein levels of IFN-γ and TNF-α in CCNVs and SCCNVs. **G)** Coomassie blue staining of lysates of B16F10 cancer cells, senescence-induced B16F10 cancer cells, CCNVs and SCCNVs. ns = Not significant. Statistical significance was calculated by Student's t-tests. * $P < 0.05$ versus CCNV.

3.2.2. In vitro dendritic cell maturation by SCCNVs

Next, I investigated whether SCCNV can promote DC maturation in vitro. SCCNV-treated DCs showed significantly higher mRNA levels of IL-6 and IL-12p40 (DC maturation markers) than CCNV-treated DCs, indicating that SCCNVs stimulate DC maturation (Figure 3.4A). CCNVs did not stimulate sufficient DC maturation since there was no difference in the mRNA levels of IL-6 and IL-12p40 between PBS and CCNV groups. FACS analysis of CD86, CD80 and MHC class I on DCs confirmed DC maturation stimulated by SCCNVs (Figure 3.4B). In addition, siRNA-SCCNVs were produced from B16F10 cancer cells that were treated with doxorubicin and transfected with siRNAs for IFN-γ and TNF-α. The siRNA transfection induced knock-down of IFN-γ and TNF-α in doxorubicin-treated B16F10 cancer cells (Figure 3.4C). siRNA-SCCNVs were less effective for DC maturation than SCCNVs (Figure 3.4D). These data indicate that enhanced DC maturation by SCCNV treatment is due to IFN-γ and TNF-α contained in SCCNVs. This suggests that significant portion of the stimulatory effect of SCCNVs on DC maturation is due to TNF-α and IFN-γ delivered by SCCNVs.

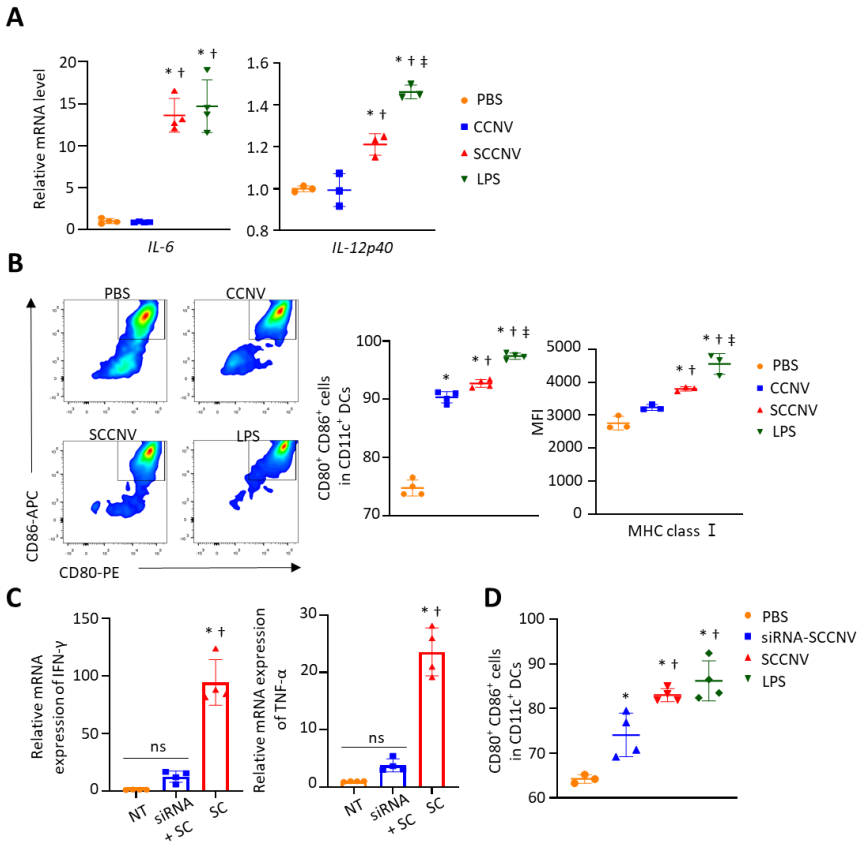

Figure 3.4 Effective DC maturation in vitro by SCCNVs. A) mRNA levels of DC maturation markers (IL-6 and IL-12p40) in BMDCs treated with PBS, CCNV, SCCNV, or LPS for 4 h in vitro, as evaluated by qRT-PCR. n = 3-4. **B)** Representative flow cytometry plot and percentage of maturation marker (CD80, CD86, MHC class I) positive cells in BMDCs treated with PBS, CCNV, SCCNV, or LPS for 24 h in vitro, evaluated by flow cytometric analysis. n = 4. **C)** siRNA transfection of senescent induction in B16F10 cells**. D)** Effect of siRNA-SCCNVs on DC maturation for 24 h, as evaluated by flow cytometric analysis. siRNA-SCCNVs are nanovesicles derived from senescent cancer cells transfected with siRNA for

IFN-γ and TNF-α. n = 4. In (B), (D), LPS was used as the positive control. Data represent mean ± SD. Statistical significance was calculated by Student's t-tests or one-way ANOVA with Tukey's significant difference multiple comparisons.* $P < 0.05$ versus PBS, versus NT in (C); † $P < 0.05$ versus CCNV in (A), (B), versus siRNA+SC in (C), versus siRNA-SCCNV in (D); ‡ $P < 0.05$ versus SCCNV in (A), (B). ns = Not significant.

3.2.3. In vivo dendritic cell maturation by SCCNVs

Ex vivo imaging 24 hrs after intradermal injection of fluorescently labeled SCCNVs or CCNVs showed that SCCNV migration to draining lymph node was significantly higher than that of CCNV (Figure 3.5A). This result may be attributed to the fact that SCCNV uptake by immature DCs stimulates DC maturation, leading to subsequent migration of mature DCs to draining lymph node, while CCNV uptake does not stimulate DC maturation. To investigate the in vivo maturation of DCs, DCs in the draining lymph node were analyzed three days after intradermal injection of SCCNVs. DCs harvested from SCCNV-injected mice showed higher expression of CD86 and MHC class I (Figure 3.5B), revealing that SCCNVs facilitated DC maturation in vivo. Seven days after intradermal injection, DC population in draining lymph nodes was significantly larger in SCCNV injection group than in CCNV or PBS injection groups (Figure 3.5C). The mRNA level of CCR7, a marker related to DC migration to secondary lymphoid organs, was significantly increased in SCCNV injection group compared to CCNV or PBS injection groups (Figure 3.5D).

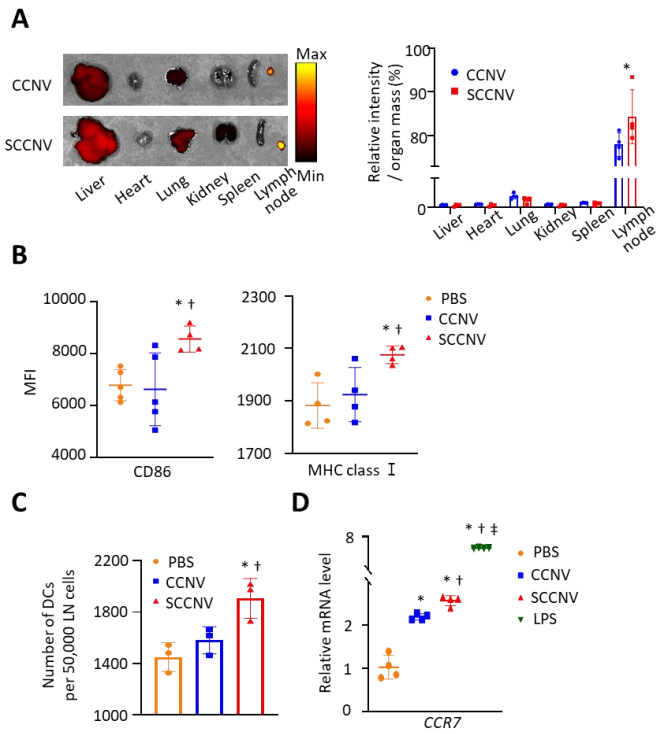

Figure 3.5 Effective homing of SCCNVs to lymph node and DC maturation in vivo. A) Ex vivo imaging 24 h after intradermal injection of fluorescently labeled CCNVs and SCCNVs. Relative fluorescence was divided by organ mass. n = 4. **B)** Maturation marker expressions in dendritic cells in draining lymph node 3 days after intradermal injection of PBS, CCNVs, or SCCNVs, as evaluated by flow cytometric analysis. n = 4-5. **C)** Number of dendritic cells in draining lymph node 7 days after intradermal injection of PBS, CCNVs, or SCCNVs, as evaluated by flow cytometric analysis. n = 3. **D)** mRNA level of CCR7, a representative marker of DC migration to secondary lymphoid organ, in BMDCs treated with PBS, CCNV, SCCNV, or LPS for 24 h in vitro. n =4. Statistical significance was calculated by one-way analysis of variance (ANOVA) with

Tukey’s significant difference multiple comparisons. * $P < 0.05$ versus CCNV in (A); versus PBS in (B)-(D). † $P < 0.05$ versus CCNV. ‡ $P < 0.05$ versus SCCNV.

3.2.4. Antigen specific T cell activation by SCCNVs

Given that SCCNVs stimulate DC maturation in vivo, I next investigated whether SCCNVs could promote the activation of tumor-specific T cells. Carboxyfluorescein succinimidyl ester (CFSE)-stained OT-1 $CD8^+$ T cells were cocultured with splenic DCs that had been pulsed with E. G7-OVA-derived CCNVs, SCCNVs or OVA peptide. The SCCNV-pulsed DCs resulted in significantly higher activation of (OT-1 transgenic mouse-derived) OVA-specific T cells than the other groups, as shown by the lower mean fluorescence intensity of CFSE-stained $CD8^+$ T cells in the SCCNV group (Figure 3.6). The positive control (the OVA peptide group) confirmed that the T cell proliferation was due to OVA pulsation of DCs. The higher T cell proliferation in SCCNV group than in OVA group may be because SCCNVs contain adjuvants (TNF-α and IFN-γ) in addition to the OVA epitope. To investigate whether SCCNVs promote T cell activation in vivo, B16F10 cancer cell-derived SCCNVs, B16F10 cancer cell-derived CCNVs, or PBS were injected intradermally into mice, and peripheral blood mononuclear cells (PBMCs) and splenocytes were collected and analyzed. After immunization, the population of $CD8^+$ T cells in the PBMCs increased significantly in SCCNV injection group (Figure 3.7A). Splenocytes isolated from immunized mice were restimulated in vitro with gp100 peptides (tumor antigen of B16F10 cancer cells). SCCNV injection group showed a higher ratio of $CD8^+$ T cells/CD3+ T cells and higher proliferation of $CD8^+$

T cells (Figure 3.7B, 3.7C). Enzyme-linked immunosorbent assay (ELISA) of supernatants from cultures of gp100-pulsed splenocytes isolated from various groups of mice revealed higher IFN-γ and TNF-α levels in SCCNV-immunized mice (Figure 3.7D), and Eyzyme-linked immunospot (ELISpot) assay showed a higher number of IFN-γ-producing, gp100-specific T cells in the spleen of the SCCNV-immunized mice than of the CCNV-immunized mice (Figure 3.7E). Together, these results indicate that SCCNV immunization more effectively stimulated the activation of vaccine antigen (gp100)-specific $CD8^+$ T cells than CCNV immunization.

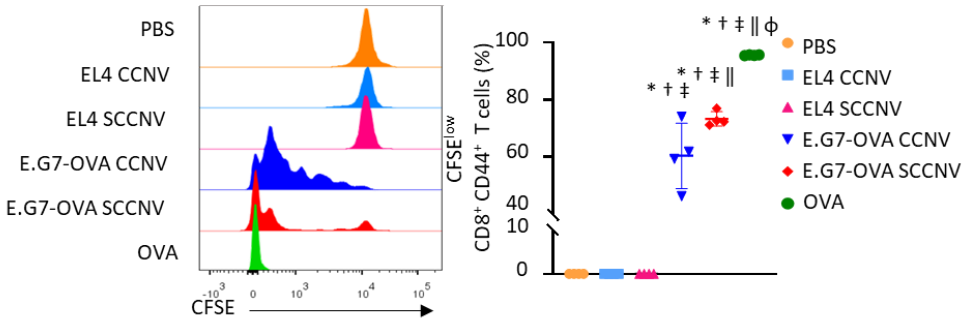

Figure 3.6 Effective activation of tumor-specific CD8+ T cells by SCCNVs in vitro.

Flow cytometric analysis for in vitro proliferation of naïve OT-I CD8+ T cells labeled with CFSE and subsequently cocultured for 72 h with splenic DCs that had been pulsed with PBS, ovalbumin peptide (OVA), CCNV or SCCNV. CCNV and SCCNV were produced from EL4-cancer cells or E.G7-OVA cancer cells. OVA was used as the positive control. * $P < 0.05$ versus PBS; † $P < 0.05$ versus EL4 cancer cell-derived CCNV; ‡ $P < 0.05$ versus EL4 cancer cell-derived SCCNV; ‖ $P < 0.05$ versus CCNV; φ $P < 0.05$ versus SCCNV.

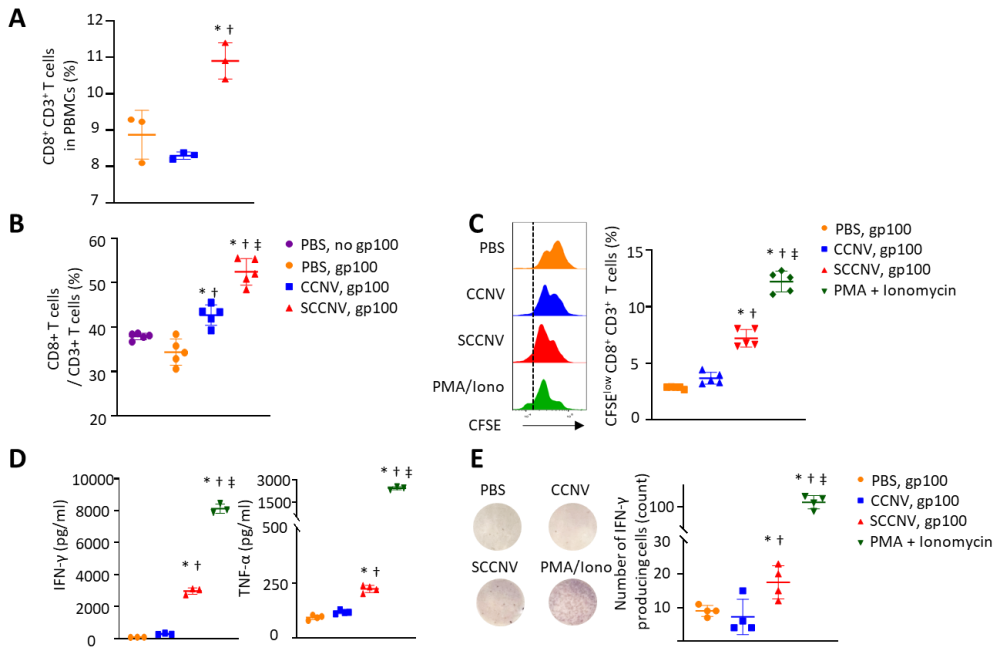

Figure 3.7 Effective activation of tumor-specific CD8+ T cells by SCCNVs in vivo.

A) Flow cytometric analysis of CD8+ T cells in PBMCs of mice immunized with intradermal injection of PBS, B16F10 cancer cell-derived CCNV, or SCCNV. **B)** Ratio of CD8+/CD3+ T cells in splenocytes harvested from mice that have been immunized with PBS, B16F10 cancer cell-derived CCNV, or SCCNV, and subsequently restimulated in vitro with gp100 peptide (the tumor antigen of B16F10 cancer cells) for 72 h. **C)** In vitro proliferation of CD8+ T cells during the restimulation of CFSE-labeled splenocytes harvested from mice that have been immunized with PBS, B16F10 cancer cell-derived CCNV, or SCCNV. PMA/Ionomycin (T cell activation-inducing agents) served as the positive control. **D)** Levels of IFN-γ and TNF-α, both of which are CD8+ T cell activation markers, in the

culture medium following the in vitro restimulation of the splenocytes. The levels of IFN-γ and TNF-α were evaluated with ELISA. **E)** ELISpot analysis of splenocytes harvested from mice immunized with various agents. Number of IFN- γ-producing cells per well were evaluated (n = 4). Statistical significance was calculated by one-way ANOVA with Tukey's significant difference multiple comparisons. * $P < 0.05$ versus PBS in (A), (C)-(E); versus PBS, no gp100 in (B). † $P < 0.05$ versus CCNV in (A), (C)-(E); versus PBS, gp100 in (B). ‡ $P < 0.05$ versus CCNV, gp100 in (B); versus SCCNV in (C)-(E).

3.2.5. In vivo tumor challenge of SCCNVs in melanoma model

Next, I investigated whether SCCNV can suppress tumor growth in prophylactic and therapeutic melanoma mouse models. in the prophylactic model, mice that underwent immunization were challenged with B16F10 melanoma (Figure 3.8A**).** SCCNV immunization inhibited tumor growth more effectively and resulted in a significantly higher survival rate than CCNV or PBS immunization (Figure 3.8B, 3.8C). SCCNVs were injected intradermally into B16F10 tumor-bearing mice (Figure 3.9A). SCCNVs significantly suppressed tumor growth in vivo and improved animal survival (Figure 3.9B, 3.9C). Terminal deoxynucleotidyl transferase dUTP nick end labeling (TUNEL) assay showed a significantly higher density of apoptotic cells in tumor tissues in SCCNV-immunized group (Figure 3.9D). Immunohistochemistry (IHC) staining and tumor infiltrating lymphocyte (TIL) analysis of tumor tissues showed significantly higher densities of activated (IFN-γ- or TNF-α-positive) cytotoxic T cells in SCCNV-immunized group (Figure 3.10A). Moreover, TIL analysis and IHC staining showed that regulatory T cell density was significantly lower in SCCNV-immunized group, indicating a proinflammatory microenvironment in SCCNV-immunized group (Figure 3.10B).

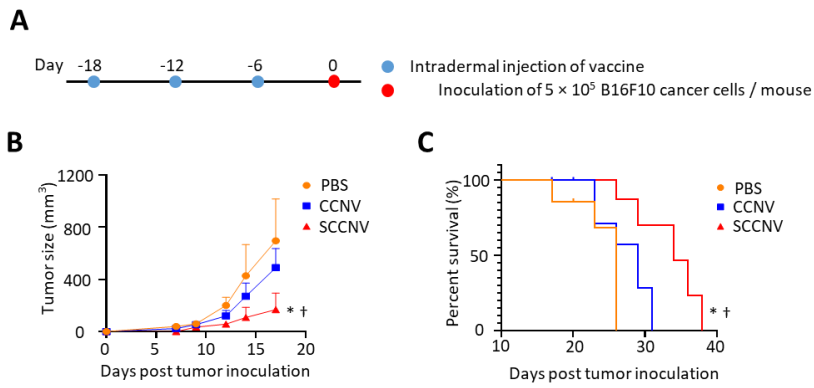

Figure 3.8 Prophylactic tumor model of SCCNVs.

A) Timeline of vaccination and prophylactic tumor modeling for (B) and (C). **B)** Tumor growth profile. n = 5. **C)** Animal survival rate. n = 5. Statistical significance was calculated by log rank (Mantel–Cox) test or by two-way ANOVA with Bonferroni post-tests. * $P < 0.05$ versus PBS; † $P<0.05$ versus CCNV.

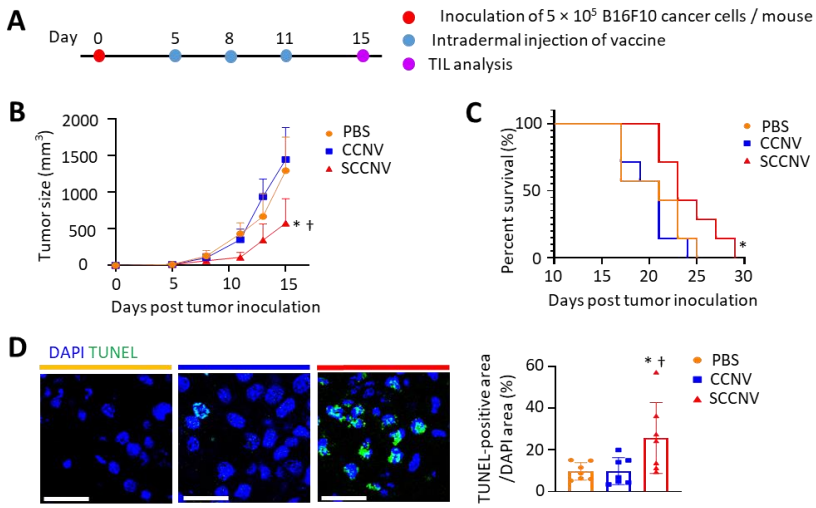

Figure 3.9 Therapeutic efficacy of SCCNV in a therapeutic melanoma murine model.

A) Timeline of therapeutic tumor modeling and vaccination for (B)-(D). **B)** Tumor growth profile. n = 6. **C)** Animal survival rate. n = 6. **D)** TUNEL assay of tumor tissues retrieved on day 15. n = 7. Scale bars = 100 μm. Statistical significance was calculated by log rank (Mantel–Cox) test, one-way ANOVA with Tukey's significant difference multiple comparisons or by two-way ANOVA with Bonferroni post-tests. * $P < 0.05$ versus PBS; † $P<0.05$ versus CCNV.

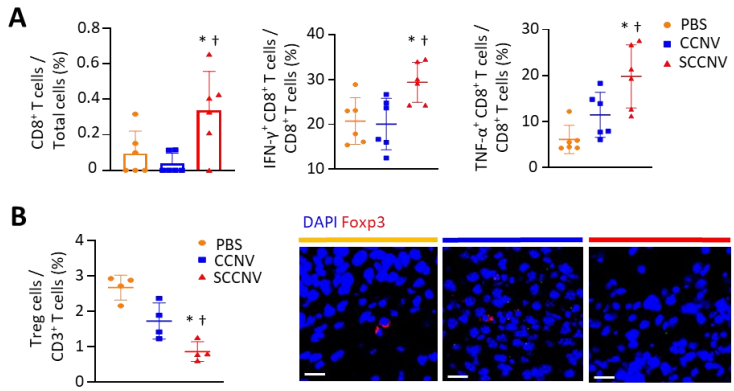

Figure 3.10 Immunohistochemistry (IHC) staining and tumor infiltrating lymphocyte (TIL) analysis of SCCNV-treated mice.

A) Immunohistochemistry for CD8+ T cells in tumor tissues, and flow cytometric TIL analysis of tumor tissues retrieved on day 15. n = 6. **B)** Percentage of Treg cells from the flow cytometric TIL analysis (n = 4) and immunohistochemistry for Foxp3 in tumor tissues retrieved on day 15. Scale bars = 50 μm. Statistical significance was calculated by one-way ANOVA with Tukey's significant difference multiple comparisons. * $P < 0.05$ versus PBS; † $P<0.05$ versus CCNV.

3.2.6. In vivo tumor challenge of SCCNVs in lung metastasis model in combination of aPD-L1 antibody

Next, I investigated whether SCCNV injection can suppress the metastatic growth of 4T1-Luc breast cancer and anti-programmed death-ligand 1 (PD-L1) antibodies were administered for combination therapy (Figure 3.11A). Live bioluminescence images of metastatic tumor-bearing mice revealed that SCCNV vaccination significantly suppressed lung metastasis (Figure 3.11B, 3.11C). Lung metastasis visualized with India ink staining confirmed the results of live bioluminescence imaging (Figure 3.11D). Importantly, SCCNV monotherapy showed a therapeutic outcome similar to that of anti-programmed death-ligand 1 (PD-L1) antibody therapy at a clinical dose. SCCNV vaccination successfully synergized with anti-PD-L1 antibody, which prevented inactivation of tumor-reactive T cells in the immunosuppressive tumor microenvironment (Figure 3.11B-D).

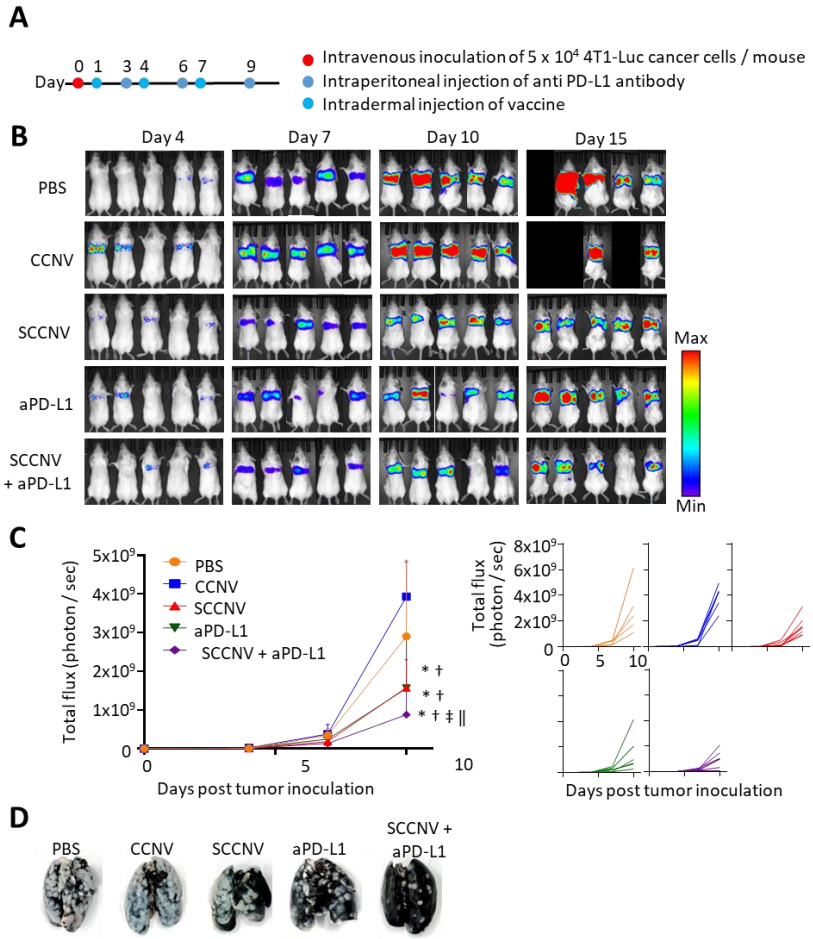

Figure 3.11 Inhibition of tumor metastasis by SCCNV injection in murine models.

A) Timeline of metastasis modeling of 4T1-Luc tumor and vaccination. **B)** Representative bioluminescence images and **C)** luminescence flux showing tumor metastasis to lung in 4T1-Luc tumor-inoculated mice at various time points. n = 5 - 6. **D)** Images of lungs harvested at day 15 and stained with India ink. Tumor nodules were stained in white, and normal lung tissues were stained in black. Statistical significance was calculated by two-way

ANOVA with Holm-Sidak post-tests. * $P < 0.05$ versus PBS; † $P < 0.05$ versus CCNV, ‡ $P < 0.05$ versus SCCNV, ‖ $P < 0.05$ versus aPD-L1.

3.2.7. In vivo tumor challenge of SCCNVs in post-surgery model

Finally, I investigated whether SCCNV vaccination can inhibit tumor recurrence in two post-surgery models of B16F10 melanoma and 4T1-Luc breast cancer. When melanoma tumor volume reached ~500 mm^3, the tumor tissues were removed, and the mice were vaccinated with B16F10 cell-derived SCCNVs (Figure 3.12A). SCCNV vaccination inhibited tumor recurrence more effectively (Figure 3.12B) and showed significantly higher survival rates (Figure 3.12C) than PBS or CCNV injection. TUNEL assay showed that SCCNV injection resulted in a significantly higher density of apoptotic cells in tumor tissues (Figure 3.12D). Additionally, in 4T1-Luc breast cancer model, SCCNV vaccination inhibited tumor recurrence more effectively than PBS or CCNV injection (Figure 3.12A, 3.12B).

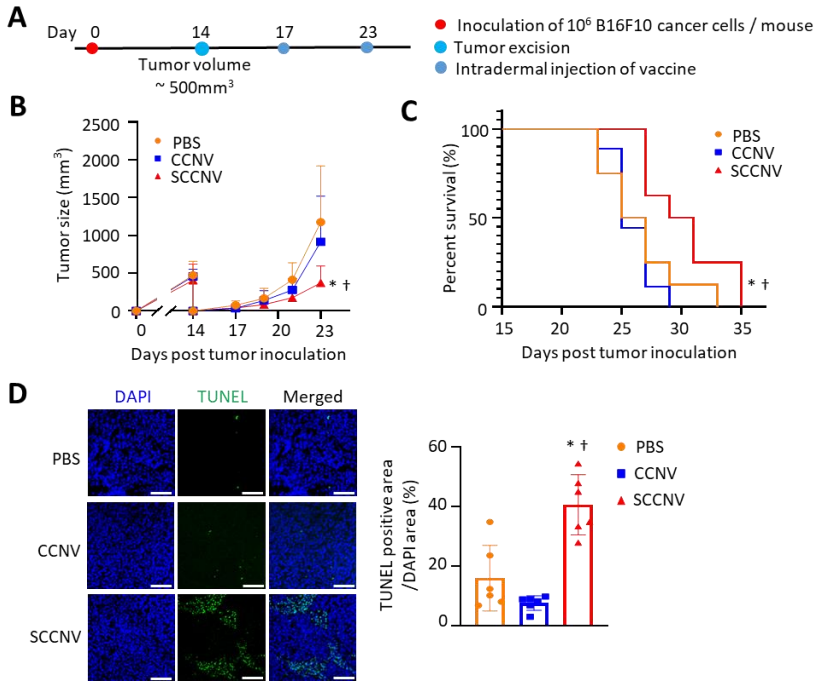

Figure 3.12 Post-surgery recurrence inhibition of melanoma tumor by SCCNV injection in murine model.

A) Timeline of post-surgery recurrence of B16F10 tumor model. **B)** Tumor growth profile. n = 13. **C)** Animal survival rate. n = 8. **D)** TUNEL assay of tumor tissues retrieved on day 27. n = 6. Scale bars = 100 μm. * $P < 0.05$ versus PBS; † $P<0.05$ versus CCNV.

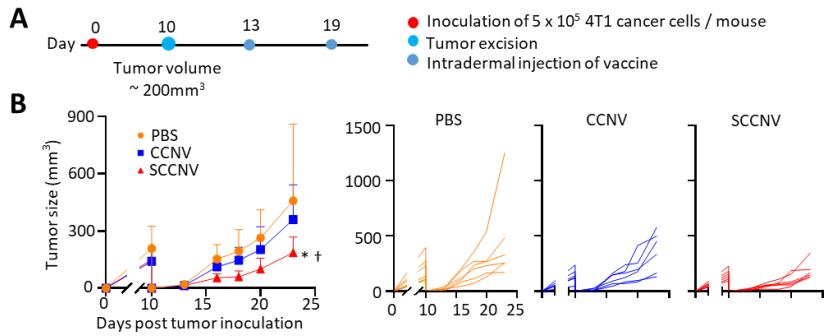

Figure 3.13 Post-surgery recurrence inhibition of 4T1 breast tumor by SCCNV injection in murine model.

A) Timeline of post-surgery recurrence of 4T1 tumor model. **B)** Tumor growth profile. n = 6. Statistical significance was calculated by two-way ANOVA with Bonferroni post-tests. * $P < 0.05$ versus PBS; † $P<0.05$ versus CCNV.

3.2.8. Discussion

As exosomes secreted from cancer cells in the TME may stimulate tumor growth by mediating crosstalk between cancer cells and immune cells in the TME[69], and SCCNVs may be similar to cancer cell-derived exosomes in terms of composition, size, and surface charge.[16] However, intradermal injection of SCCNVs did not cause tumor growth stimulation because SCCNVs were injected subcutaneously and internalized to DCs in the tumor-free region, which prevents crosstalk between SCCNVs and immune cells in the TME. Furthermore, unlike cancer cell-derived exosomes or CCNVs, SCCNVs contain proinflammatory cytokines (IFN-γ and TNF-α) that induce antitumoral microenvironments upon interaction with the TME.

In addition, SCCNVs were chosen for TCV to deliver various tumor antigens. Tumor lysates, which may have similar composition to cancer cell derived nanovesicles, can also be used as a potential TCV to deliver tumor antigens, but tumor lysate vaccination generally results in low-efficiency DC activation and, in turn, low antitumor immunity.[70] In contrast, SCCNVs can deliver tumor antigens and proinflammatory cytokines (IFN-γ and TNF-α) simultaneously to DCs, leading to higher efficiency of DC activation (Figure 3B, 3C, and 4B). The effective DC activation led to effective activation of tumor antigen-specific T cells (Figure 5C-F and 6E) and tumor inhibition in various mouse tumor models, including a prophylactic model (Figure 6A-F), primary tumor model (Figure 6G-I), metastasis model

(Figure 7) and postsurgery tumor recurrence model (Figure 8). These results show the potential of SCCNVs as TCV.

SCCNVs may be clinically feasible for personalized TCV. In this present study, I treated mouse tumor models with SCCNVs derived from in vitro senescence-induced cancer cell lines, because these immortalized cell lines preserve most of the antigens in short period.[71] The heterogeneity of tumor cells and the difficulty of neoantigen identification make tumor treatment difficult. In contrast, SCCNVs obtained from autologous tumor tissues would provide a patient-specific spectrum of tumor antigens with no need of neoantigen identification. In addition, liquid tumors, such as acute myeloid leukemia, have a small chance of being treated with immunotherapy due to their limited identification of tumor antigens and low response rate to immune checkpoint blockades.[10,72] SCCNV therapy can be applied for liquid tumors by collecting tumor cells from the patient's blood and delivering patient-specific tumor antigens through SCCNVs. SCCNVs may elicit systemic antitumor immunity against liquid tumors, as shown in the inhibition of metastatic tumor growth by SCCNVs (Figure 7). For solid tumors, SCCNVs as personalized TCVs could be prepared from autologous tumor tissues removed during surgery in end-stage cancer patients in which surgical removal of tumor tissues may be necessary. In addition, SCCNVs could be used to remove metastatic cancer cells (Figure 7) and prevent tumor recurrence (Figure 8) in end-stage cancer patients in which metastasis or tumor recurrence is often observed.

Currently, several clinical trials are ongoing to evaluate the efficacy of TCVs with neoantigens in the form of peptides (NCT03639714, NCT03223103 and NCT02721043), mRNA (NCT04163094) and DNA (NCT04015700 and NCT04251117). However, the development of TCVs employing neoantigens is limited by difficulty, labor intensiveness, and high cost in accurate prediction of immunogenic neoantigens and by patient-to-patient variations in neoantigens. Only a small fraction (~1-2%) of mutations in cancer cells induce antitumor immune responses[56], making it difficult to accurately predict clinically effective neoantigens. Only a small number of neoantigens are shared between cancer patients[8], making it hardly feasible to screen neoantigens for individual patients. The processes of exploring suitable neoantigens for individual patients would be laborious and costly. TCV therapy employing a single neoantigen may fail for tumors that undergo ceaseless mutations, modulate the expression of neoantigens, and consequently evade recognition by vaccine-activated T cells.[73] In contrast, SCCNVs produced from autologous cancer cells avoid labor-intensive and time-consuming processes of identification and prediction of immunogenic neoantigens for individual patients, are free from the concern of patient-to-patient variations in neoantigens, contain a broad spectrum of patient-specific neoantigens, and can avoid tumor immune escape.

On the other hand, there is an obvious limitation to address for SCCNVs. As whole tumor cell derived nanovesicles, SCCNVs may deliver tumor non-specific antigens, which is expressed in normal cells. Therefore

SCCNVs may elicit immunity against normal cells, resulting in autoimmune disorders. In clinical trial of whole tumor vaccines, there was no autoimmune disorders at life-threatening level, as normal cell antigens are usually ignored by central tolerance of immune systems[74,75]. But this central tolerance often hinders immunogenicity of tumor vaccines, so there is a need to find a way to efficiently upregulate tumor vaccine immunogenicity.

In conclusion, this study suggests SCCNV as a potential personalized TCV strategy. SCCNVs prepared from autologous (possibly heterogeneous) cancer cells can deliver a broad spectrum of patient-specific neoantigens and safe adjuvants and effectively activate tumor-reactive T cells. Immune checkpoint blockades that prevent T cell exhaustion in the immunosuppressive TME can synergistically collaborate with tumor-reactive T cells activated by SCCNVs to inhibit tumor growth (Figure 7). SCCNVs may show clinical benefit since SCCNVs showed an efficacy similar to that of immune checkpoint blockade therapy (anti-PD-L1 antibody) in thisanimal study (Figure 7).

3.3 Experimental sectino

3.3.1. Cell culture

B16F10 cells were purchased from American Type Culture Collection (ATCC, VA, USA) and were cultured in Dulbecco's modified Eagle's medium (DMEM) (Gibco, NY, USA) supplemented with 10% (v/v) FBS and 1% (v/v) PS. E. G7-OVA cells, a variant of the EL4 cell line that expresses full-length OVA, were a gift from Professor Junsang Doh, Seoul National University, Seoul, Korea. E. G7-OVA cells were cultured in RPMI 1640 (Gibco) containing 10% (v/v) FBS, 1% (v/v) PS, 10 mM HEPES, 1.0 mM sodium pyruvate, 0.05 mM β-mercaptoethanol and 0.04 μg/ml of G-418 antibiotics (Roche). 4T1 cells were purchased from ATCC and cultured in RPMI 1640 containing 10% (v/v) FBS and 1% (v/v) PS. Primary T cells were isolated from spleens of 6-week-old female C57BL/6 mice (Orient Bio, Gyeonggi, Korea) using a MojoSort™ Mouse CD8 T Cell Isolation Kit (Biolegend) according to the manufacturer's protocol. Cells were then cultured in RPMI 1640 supplemented with 10% (v/v) FBS, 1% (v/v) PS, 1% (v/v) GlutaMAX (Gibco), 10 mM HEPES, 1 mM sodium pyruvate and 55 μM 2-mercaptoethanol.

3.3.2. Preparation of SCCNVs

SCCNVs were produced from cancer cell lines. For senescent induction, 0.1 μM doxorubicin hydrochloride (doxorubicin HCl, Sigma Aldrich, MO, USA) was added to cell culture medium for 24 hrs. Then, cells were washed with PBS, changed to doxorubicin-free media and cultured for an additional four days[76,77]. Senescence-induced cancer cells were detached from cell culture plate using trypsin-EDTA, washed with PBS and serially extruded through polycarbonate membrane filters (Whatman, UK) with pore sizes of 1 μm, 400 nm and 200 nm using a mini-extruder (Avanti Polar Lipids, AL, USA) to obtain nanovesicles as previously reported. [12] To reload antigen peptides, which might have been dissociated from MHC class I of nanovesicles, on the MHC class I, pH of the nanovesicle-containing solution was adjusted to 5.5 by sodium acetate buffer for 30 min and then neutralized by Tris-HCl buffer.[78,79] Nanovesicles were then centrifuged at 30,000 g for 1 hrs at 4 °C. Protein concentration of isolated SCCNVs was quantified using Bradford reagent (Sigma Aldrich) according to the manufacturer's protocol.

3.3.3. Optimization of senescence induction

B16F10 cells were treated with doxorubicin HCl at concentrations of 0, 0.1, 0.5, and 1 μM. To evaluate senescence, cells were stained with a senescence-associated β-galactosidase (SA-β-gal) staining kit (Cell Signaling Technology, MA, USA) according to the manufacturer's protocol. To evaluate cytotoxicity of doxorubicin HCl, a Cell Counting Kit-8 (CCK-8, DoGenBio, Seoul, Korea) was used according to the manufacturer's protocol.

3.3.4. Characterization of SCCNVs

The size distributions of SCCNVs were assessed using dynamic light scattering (Zetasizer Nano ZS, Malvern Panalytical, UK). For the evaluation of colloidal stability of SCCNVs in a 30% FBS-containing buffer, the hydrodynamic diameter of SCCNVs was detected with a Zetasizer at various time points. The morphology of SCCNVs was evaluated with a JEM-2100 transmission electron microscope (JEOL, Japan) installed at the National Center for Inter-university Research Facilities (NCIRF) at Seoul National University. Relative mRNA expression levels of IFN-γ and TNF-α were determined with qRT–PCR analysis. mRNA from cancer cells or nanovesicles was extracted using QIAzol Lysis Reagent (Qiagen, CA, USA). RNA from each group was used for cDNA synthesis using PCR PreMix (Bioneer, Daejeon, Korea). SYBR green-based qRT–PCR was performed with TOPreal™ qPCR 2X PreMIX (Enzynomics, Daejeon, Korea). The cycling conditions were as follows: initial denaturation at 95 °C for 15 min, followed by 60 cycles at 95 °C for 10 s, 60 °C for 15 s and 72 °C for 30 s. The expression of each gene was normalized to GAPDH expression. Protein levels of IFN-γ and TNF-α were evaluated with western blot using anti-mouse IFN-γ antibody, anti-mouse TNF-α antibody (Bioss, MA, USA) and anti-mouse GAPDH antibody (Invitrogen, CA, USA). GAPDH was used as the control protein. For Coomassie blue staining, proteins in lysates of normal B16F0 cells, senescent B16F10 cells, CCNVs and SCCNVs were

separated using SDS–PAGE, and polyacrylamide gel was stained with Coomassie blue using PageBlue™ Protein Staining Solution (Thermo Scientific, MA, USA) to visualize the proteins. Amounts of IFN-γ and TNF-α was detected by analyzing lysates of CCNVs and SCCNVs by ELISA kit (Biolegend). Calculated amounts of IFN-γ and TNF-α were divided by total protein amount to get amounts of IFN-γ and TNF-α per 1 ug of SCCNVs.

3.3.5. Isolation of BMDCs

BMDCs were isolated as previously described.[80] Briefly, 6-week-old C57BL/6 mice was sacrified and the femurs were isolated from the hind limb. The bones were flushed with PBS using syringes to isolate bone marrow cells. Red blood cell lysis buffer was added. After centrifugation, mononuclear bone marrow cells were cultured in dishes containing 10 mL of differentiation medium consisting of RPMI 1640 medium supplemented with 20 ng/mL GM-CSF (R&D Systems, MN, USA) and 10% (v/v) FBS. After 3 days, 5 mL of fresh differentiation medium was added to the dishes. Differentiated BMDCs were collected on day 10.

3.3.6. In vitro DC maturation

For in vitro DC maturation analysis, 5×10^5 BMDCs were plated on each well of 6-well plates prior to SCCNV treatment. To investigate SCCNV uptake by DCs, 20 μg of CCNV or SCCNV was stained with 1,1'-dioctadecyl-3,3,3',3'-tetramethylindocarbocyanine perchlorate (DiI, Invitrogen) according to the manufacturer's protocol. BMDCs were treated with DiI-stained CCNVs or SCCNVs and analyzed with FACS using a BD Canto-II flow cytometer (BD Sciences, CA, USA). To determine mRNA levels in DCs, BMDCs were treated with 20 μg of CCNVs or SCCNVs for 4 hrs. Treatment with 100 ng/ml lipopolysaccharide (LPS, Sigma Aldrich, MO, USA) was used as the positive control. Then, cells were lysed with QIAzol lysis reagent (QIAgen, CA, USA) for mRNA extraction. Relative mRNA levels of IL-6, IL-12p40 and CCR7 were evaluated through qRT–PCR. The expression of each gene was normalized by GAPDH expression. For detection of surface protein expression on BMDCs, BMDCs were treated with 20 μg of CCNVs or SCCNVs for 24 hrs. Then, BMDCs were detached with trypsin-EDTA and stained with the following antibodies: APC-Cy7 anti-mouse CD11c antibody, PE anti-mouse CD80 antibody, APC anti-mouse CD86 antibody and FITC anti-mouse MHC class I antibody (Biolegend, CA, USA). Fluorescently stained DCs were analyzed with a BD Canto-II flow cytometer (BD Sciences). FACS data were analyzed using

FlowJo software (Tree Star Inc., OR, USA). For proinflammatory cytokine-induced maturation of DCs, BMDCs were treated with CCNV and recombinant proteins TNF-α (100 ng/ml) and IFN-γ (20 ng/ml) (Biolegend)[81,82]. Then, BMDCs were detached and stained with the following antibodies: APC-Cy7 anti-mouse CD11c antibody, PE anti-mouse CD80 antibody and APC anti-mouse CD86 antibody (Biolegend).

3.3.7. In vivo imaging of SCCNVs

For in vivo imaging of the intradermally injected nanovesicles, CCNVs or SCCNVs were stained with VivoTrack 680 (Perkin Elmer, MA, USA) according to the manufacturer's protocol. VivoTrack-stained CCNVs or SCCNVs (20 μg) were suspended in 50 μl PBS and intradermally injected into the right flank of mice (n = 4 animals). To monitor the biodistribution of injected SCCNVs, the mice were sacrificed 24 hrs after the injection. Five major organs (heart, lung, liver, kidney and spleen) and lymph nodes near the injection site were retrieved. Fluorescence signals were acquired using IVIS spectrum computed tomography (Perkin Elmer) at 680 nm excitation and quantified using Living Image 3.1 software. Fluorescence intensity of each organ or lymph node was normalized to the sum of intensities of the organs and tumors in each group.

3.3.8. In vivo DC maturation

For analysis of in vivo DC maturation, PBS, CCNVs or SCCNVs were intradermally injected into the right flank of 6-week-old C57BL/6 mice. Three days after injection, right inguinal lymph node was harvested from the mice, minced, and passed through a 70-μm pore filter. The separated single cells were stained with the following antibodies: PE anti-mouse CD11c antibody, APC anti-mouse CD86 antibody and FITC anti-mouse MHC class I antibody (Biolegend). Fluorescently stained cells were analyzed with a BD Canto-II flow cytometer (BD Sciences). FACS data were analyzed using FlowJo software (Tree Star Inc.). To investigate DC accumulation in lymph nodes after intradermal injection of PBS, CCNVs or SCCNVs, right side inguinal lymph nodes were harvested 7 days after intradermal injection. Then, the lymph nodes were minced and passed through a 70-μm pore filter. The separated single cells were stained with a PE anti-mouse CD11c antibody, and the number of DCs was obtained through FACS analysis.

3.3.9. In vitro T cell proliferation analysis

OVA-specific $CD8^+$ T cells harvested from OT-1 transgenic mice were used for in vitro T cell proliferation assay. Briefly, the lymph nodes and spleen of OT-1 mice were harvested, minced, and passed through a 70-μm pore filter. Then, $CD8^+$ T cells were isolated using a Mojosort $CD8^+$ T cell isolation kit (Biolegend) according to the manufacturer's protocol. Isolated OT-1 $CD8^+$ T cells were stained with a CFSE cell division tracker kit (Biolegend) and cocultured with splenocytes isolated from wild-type C57BL/6 mice that contained splenic DCs. Then, 1 μg/ml CCNVs and SCCNVs, which were produced from OVA-expressing E. G7-OVA cancer cells, were added to the cultures. One microgram/ml OVA epitope peptide (257-264, ANASPEC, CA, USA) was used as the positive control. After three days of culture, cells were harvested and stained with BV421 anti-mouse CD3 antibody and PE-Cy7 anti-mouse CD8 antibody (Biolegend). Then, the percentages of $CFSE^{low}$ $CD3^+$ $CD8^+$ T cells were calculated.

3.3.10. Mouse immunization model

To investigate the immune responses of SCCNVs, C57BL/6 mice were intradermally injected with PBS, CCNVs or SCCNVs three times every 6 days. Three days after injection, blood was harvested from the immunized mice through retro-orbital bleeding, and red blood cells and lymphocytes were collected by centrifugation at 3,000 g for 30 min. Then, the red blood cells were lysed using RBC lysis buffer (Gibco). The lymphocytes were then stained with BV421 anti-mouse CD3 antibody, APC anti-mouse CD4 antibody and PE-Cy7 anti-mouse CD8 antibody (Biolegend) and analyzed with a BD Canto-II flow cytometer (BD Sciences). Six days after the last immunization, splenocytes were harvested from the mice and restimulated with 1μg/ml gp100 peptides, the antigen epitope of B16F10 cancer cells. After three days of culture, $CD8^+$ T cells in the splenocytes were stained with BV421 anti-mouse CD3 antibody, APC anti-mouse CD4 antibody and PE-Cy7 anti-mouse CD8 antibody (Biolegend), and culture supernatants were analyzed with IFN-γ and TNF-α ELISA kits (Biolegend). For CFSE staining, splenocytes were stained with CFSE first and then restimulated with gp100 peptides. After three days, splenocytes were stained with anti-mouse CD3 antibody and PE-Cy7 anti-mouse CD8 antibody (Biolegend), and analyzed by BD Canto II, detecting $CFSE^{low}$ CD3+ CD8+ T cells.

3.3.11. In vivo prophylactic model

Six-week-old C57BL/6 mice were randomly divided into three groups, anesthetized with rumpun (10 mg/kg) and ketamine (100 mg/kg) and intradermally injected with PBS, CCNVs or SCCNVs (20 μg of nanovesicles in 50 μl of PBS) once a week for three weeks. Six days after the last immunization, the mice were injected with B16F10 cancer cells (5×10^5 cells in 100 μL PBS per mouse) subcutaneously into the right flank. Tumor sizes were measured every three days using a digital caliper and computed according to the ellipsoidal calculation: V = 0.5 × (longest diameter) × (shortest diameter). Survival of the mice was monitored for 40 days. The mice bearing tumors exceeding 2,500 mm^3 in size were euthanized with CO_2 inhalation.

3.3.12. In vivo tumor challenge model

Six-week-old C57BL/6 mice were anesthetized with rumpun (10 mg/kg) and ketamine (100 mg/kg) and injected with B16F10 cancer cells (5×10^5 cells in 100 μL of PBS per mouse) subcutaneously into the right flank. On Days 5, 8, and 11, the mice were intradermally injected with PBS, CCNVs or SCCNVs (20 μg of nanovesicles in 50 μl of PBS). Tumor sizes were measured every three days using a digital caliper and computed according to the ellipsoidal calculation: V = 0.5 × (longest diameter) × (shortest diameter). Survival of the mice was monitored for 30 days. The mice bearing tumors exceeding 2,500 mm^3 in size were euthanized with CO_2 inhalation.

3.3.13. Tumor-infiltrating lymphocyte analysis

Tumor-infiltrating lymphocytes were analyzed as previously described. [37,83] Briefly, four days after the last injection, the tumor masses were harvested from the euthanized mice, and the tumor masses were weighed. Then, the tumor tissues were minced and passed through a 70-μm pore filter. The separated single cells were stained with the following antibodies: anti-mouse CD3, anti-mouse CD4, anti-mouse CD8, anti-mouse Foxp3, anti-mouse IFN-γ and anti-mouse TNF-α (Biolegend). Intracellular staining of tumor infiltrating lymphocytes was conducted according to the manufacturer's protocol. The staining results were analyzed using FlowJo software (Tree Star Inc.).

3.3.14. Immunohistochemistry staining of tumor sections

Tumor tissues were fixed in 4% PFA and kept in 30% sucrose solution for one day. The fixed tissues were embedded in OCT (Scigen Scientific, CA, USA) and stored at -80 ℃. The cryopreserved tissues were sectioned at 10-μm thickness using a cryostat microtome (Leica, Germany). For Foxp3 staining, the tissue sections were washed with PBS twice, blocked, and permeabilized with 0.6% Triton X-100 and 10% donkey serum (Gibco) in PBS for 2 hrs. Then, the sections were incubated with anti-mouse Foxp3 antibodies (Biolegend) overnight at 4 ℃. The unbound antibodies were removed, and the cell nuclei were stained with DAPI for 10 min. Fluorescence images were obtained with an LSM 710 confocal microscope (Carl Zeiss). For the terminal deoxynucleotidyl transferase-mediated dUTP nick end labeling (TUNEL) assays, the tumor tissue sections were washed and stained using DeadEnd™ Fluorometric TUNEL System (Promega, WI, USA) according to the manufacturer's protocol. Images were obtained with LSM 710 (Carl Zeiss), and TUNEL-positive cell percentages were calculated using NIH ImageJ software (Bethesda).

3.3.15. In vivo toxicity of SCCNVs

C57BL/6 mice were anesthetized with rumpun (10 mg/kg) and ketamine (100 mg/kg) and intradermally injected with PBS, CCNVs or SCCNVs (20 μg of nanovesicles in 50 μl of PBS). Blood samples were obtained at various time points. Serum was obtained from the blood by centrifugation at 3,000 g for 30 min. The levels of AST, ALT, creatinine and BUN in the serum were determined with a DRI-CHEM 3500S chemistry analyzer (Fujifilm, Japan). For histological analysis, major organs (liver, lung, spleen, heart and kidney) were retrieved 14 days after the first injection. The tissues were fixed in 4% PFA overnight at 4 °C and dehydrated in 30% sucrose solution. The tissues were embedded in OCT compound (Scigen Scientific) and sectioned to a thickness of 10 μm using a cryostat microtome (Leica, Germany). The sections were stained with hematoxylin (Cancer Diagnostics, NC, USA) and eosin (BBC Biochemical, WA, USA) and imaged using an optical microscope (Olympus, Tokyo, Japan).

3.3.16. Lung metastasis tumor model

Six-week-old C57BL/6 mice were anesthetized with rumpun (10 mg/kg) and ketamine (100 mg/kg), and 5×10^4 4T1-Luc tumor cells were injected intravenously. On Days 1, 4, and 7, PBS, 4T1-Luc cancer cell-derived CCNVs or SCCNVs were intradermally injected. On Days 3, 6, and 9, 200 μg of anti-programmed death-ligand 1 (PD-L1) antibodies (BioXcell, NH, USA) was intraperitoneally injected to evaluate the synergized antitumor efficacy of SCCNVs. To obtain bioluminescence images, prior to imaging, D-luciferin potassium salt (Gold Biotechnology, MO, USA) in sterile water were injected intraperitoneally according to the manufacturer's protocol.[80] Bioluminescence images were acquired through IVIS spectrum computed tomography (Perkin Elmer), and the total flux of luminescence in lung tissues was quantified using Living Image 3.1 software. On Day 15, 15% India ink solution was injected intratracheally, and the India ink-stained lung tissues were harvested. The harvested lung tissues were washed with distilled water and fixed in Fekete's solution overnight. Then, images of the India ink-stained lung tissues were obtained, with tumor nodules visualized in white.

3.3.17. Post-surgery model tumor model

Six-week-old C57BL/6 mice were anesthetized with rumpun (10 mg/kg) and ketamine (100 mg/kg) and injected with B16F10 cancer cells (5×10^5 cells in 100 μL PBS per mouse) subcutaneously into the right flank. At Day 14, the tumor volume reached ~ 500 mm^3, the mice were anesthetized with rumpun and ketamine, and the tumor tissues were excised. At Day 17, the mice were randomly divided into three groups and intradermally injected with PBS, CCNVs or SCCNVs (20 μg of nanovesicles in 50 μl of PBS) at Day 17 and Day 23. Tumor sizes were measured every two days using a digital caliper and computed according to the ellipsoidal calculation: V = 0.5 × (longest diameter) × (shortest diameter). Survival of the mice was monitored for 35 days. The mice bearing tumors exceeding 2,500 mm^3 in size were euthanized with CO_2 inhalation. For immunohistochemistry staining of the tumor tissues, the tumor tissues were harvested at Day 27. The tumor tissues were analyzed with DeadEnd™ Fluorometric TUNEL System (Promega, WI, USA) according to the manufacturer's protocol. For the postsurgery 4T1 breast cancer model, 5×10^5 cells in 100 μL of PBS per mouse were inoculated into the right flanks of the mice. When the tumor size reached ~ 200 mm^3, the tumor tissues were excised, and PBS, 4T1 cancer cell-derived CCNV or SCCNV was injected. Tumor sizes were measured every three days.

3.3.18. Statistical analysis

Unless described otherwise, the data are presented as the mean ± standard deviation (SD). The data were analyzed through one-way analysis of variance (ANOVA) with Tukey's significant difference multiple comparisons to calculate P values for comparisons between more than two groups. Two-way ANOVA with Bonferroni's correction or Holm-Sidak post-tests was used to calculate the P values for comparisons between groups over multiple time points. The log-rank test was used to compare survival differences in the Kaplan–Meier plots using Prism software (GraphPad, CA, USA).

Chapter 4. Conclusion

Here, I proposed cell-derived nanovesicles, TCNVs and SCCNVs, for novel cancer immunotherapies, and investigated their antitumor mechanisms and in vivo efficacy in mice tumor models.

It was revealed that TCNVs well preserved $CD8^+$ T cell's characteristic, and successfully blocked PD-L1, scavenged TGF-β and delivered granzyme B to cancer cells in vitro. In vivo efficacy of TCNVs was tested in LLC mice tumor model, and both intratumoral and intravenous injection of TCNVs showed impressive tumor suppression. In addition, TCNVs did not suffer from exhaustive environment of tumor tissues. These result shows that TCNVs could be utilized as a potential treatment for immune suppressive tumors.

In vitro investigation showed that SCCNVs successfully contained cancer cell antigens and pro-inflammatory cytokines, and successfully maturated dendritic cells. Also, SCCNV injection showed highly activated antigen specific T cells and their antitumor efficacy was tested in prophylactic model, therapeutic model, lung metastasis model and post-surgery model. These in vivo model interferon-gamma (IFN-γ) and tumor necrosis factor-alpha (TNF-α).s revealed the potential of SCCNVs as an efficient cancer vaccine platform, which may be collaborated with current ICB therapy.

Altogether, cell-derived nanovesicles showed significant antitumor efficacy as novel cancer immunotherapeutics, and the clinical application of cell-derived nanovesicles is anticipated in future.

Bibliography

1 Siegel, R. L., Miller, K. D., Fuchs, H. E. & Jemal, A. Cancer statistics, 2022. *CA: a cancer journal for clinicians* **72**, 7-33 (2022).

2 Kroemer, G. & Zitvogel, L. Immune checkpoint inhibitors. *Journal of Experimental Medicine* **218** (2021).

3 Waldman, A. D., Fritz, J. M. & Lenardo, M. J. A guide to cancer immunotherapy: from T cell basic science to clinical practice. *Nature Reviews Immunology* **20**, 651-668 (2020).

4 Ghorashian, S. *et al.* Enhanced CAR T cell expansion and prolonged persistence in pediatric patients with ALL treated with a low-affinity CD19 CAR. *Nature medicine* **25**, 1408-1414 (2019).

5 Fry, T. J. *et al.* CD22-targeted CAR T cells induce remission in B-ALL that is naive or resistant to CD19-targeted CAR immunotherapy. *Nature medicine* **24**, 20 (2018).

6 Shin, S. *et al.* Tumor Microenvironment Modulating Functional Nanoparticles for Effective Cancer Treatments. *Tissue Engineering and Regenerative Medicine*, 1-15 (2021).

7 Luchner, M., Reinke, S. & Milicic, A. TLR agonists as vaccine adjuvants targeting cancer and infectious diseases. *Pharmaceutics* **13**, 142 (2021).

8 Peng, M. *et al.* Neoantigen vaccine: an emerging tumor immunotherapy. *Molecular cancer* **18**, 1-14 (2019).

9 Yang, J. C. & Rosenberg, S. A. Adoptive T-cell therapy for cancer. *Advances in immunology* **130**, 279-294 (2016).

10 Mardiana, S. & Gill, S. CAR T cells for acute myeloid leukemia: state of the art and future directions. *Frontiers in oncology* **10**, 697 (2020).

11 Esfahani, K. *et al.* A review of cancer immunotherapy: from the past, to the present, to the future. *Current Oncology* **27**, 87-97 (2020).

12 Jang, S. C. *et al.* Bioinspired exosome-mimetic nanovesicles for targeted delivery of chemotherapeutics to malignant tumors. *ACS nano* **7**, 7698-7710 (2013).

13 Rezaie, J., Feghhi, M. & Etemadi, T. A review on exosomes application in clinical trials: Perspective, questions, and challenges. *Cell Communication and Signaling* **20**, 1-13 (2022).

14 Lau, H. C. *et al.* GMP-compliant manufacturing of biologically active cell-derived vesicles produced by extrusion technology. *Journal of Extracellular Biology* **1**, e70 (2022).

15 Fu, S., Wang, Y., Xia, X. & Zheng, J. C. Exosome engineering: Current progress in cargo loading and targeted delivery. *NanoImpact* **20**, 100261 (2020).

16 Kim, H. Y. *et al.* Therapeutic efficacy-potentiated and diseased organ-targeting nanovesicles derived from mesenchymal stem cells for spinal cord injury treatment. *Nano letters* **18**, 4965-4975 (2018).

17 Neelapu, S. S. *et al.* Axicabtagene ciloleucel CAR T-cell therapy in

refractory large B-cell lymphoma. *New England Journal of Medicine* **377**, 2531-2544 (2017).

18 Brudno, J. N. & Kochenderfer, J. N. Chimeric antigen receptor T-cell therapies for lymphoma. *Nature reviews Clinical oncology* **15**, 31 (2018).

19 Shah, N. N. & Fry, T. J. Mechanisms of resistance to CAR T cell therapy. *Nature Reviews Clinical Oncology* **16**, 372-385 (2019).

20 Lord, S. J., Rajotte, R. V., Korbutt, G. S. & Bleackley, R. C. Granzyme B: a natural born killer. *Immunological reviews* **193**, 31-38 (2003).

21 Gholami, M. D., Saeedi, Y., Heydari, S., Garssen, J. & Falak, R. Exhaustion of T lymphocytes in the tumor microenvironment: significance and effective mechanisms. *Cellular immunology* **322**, 1-14 (2017).

22 Zhang, Z., Liu, S., Zhang, B., Qiao, L. & Zhang, Y. T cell dysfunction and exhaustion in cancer. *Frontiers in Cell and Developmental Biology* **8**, 17 (2020).

23 Jiang, Y., Li, Y. & Zhu, B. T-cell exhaustion in the tumor microenvironment. *Cell death & disease* **6**, e1792 (2015).

24 Freeman, G. J. *et al.* Engagement of the PD-1 immunoinhibitory receptor by a novel B7 family member leads to negative regulation of lymphocyte activation. *The Journal of experimental medicine* **192**, 1027-1034 (2000).

25 Chen, W. *et al.* Conversion of peripheral CD4+ CD25− naive T cells to CD4+ CD25+ regulatory T cells by TGF-β induction of transcription factor Foxp3. *The Journal of experimental medicine* **198**, 1875-1886 (2003).

26 Fantini, M. C. *et al.* Cutting edge: TGF-β induces a regulatory phenotype in CD4+ CD25− T cells through Foxp3 induction and down-regulation of Smad7. *The Journal of Immunology* **172**, 5149-5153 (2004).

27 Taylor, A., Verhagen, J., Blaser, K., Akdis, M. & Akdis, C. A. Mechanisms of immune suppression by interleukin-10 and transforming growth factor-β: the role of T regulatory cells. *Immunology* **117**, 433-442 (2006).

28 Gratchev, A. TGF-β signalling in tumour associated macrophages. *Immunobiology* **222**, 75-81 (2017).

29 Liu, J. *et al.* Tumor-associated macrophages recruit CCR6+ regulatory T cells and promote the development of colorectal cancer via enhancing CCL20 production in mice. *PloS one* **6**, e19495 (2011).

30 Thomas, D. A. & Massagué, J. TGF-β directly targets cytotoxic T cell functions during tumor evasion of immune surveillance. *Cancer cell* **8**, 369-380 (2005).

31 Agata, Y. *et al.* Expression of the PD-1 antigen on the surface of stimulated mouse T and B lymphocytes. *International immunology* **8**,

765-772 (1996).

32 Shresta, S., Pham, C. T., Thomas, D. A., Graubert, T. A. & Ley, T. J. How do cytotoxic lymphocytes kill their targets? *Current opinion in immunology* **10**, 581-587 (1998).

33 Barry, M. *et al.* Granzyme B short-circuits the need for caspase 8 activity during granule-mediated cytotoxic T-lymphocyte killing by directly cleaving Bid. *Molecular and cellular biology* **20**, 3781-3794 (2000).

34 Medema, J. P. *et al.* Cleavage of FLICE (caspase-8) by granzyme B during cytotoxic T lymphocyte-induced apoptosis. *European journal of immunology* **27**, 3492-3498 (1997).

35 Buschow, S. I., Anderton, S. M., Stoorvogel, W. & Wauben, M. H. Activated T cells recruit exosomes secreted by dendritic cells via LFA-1. *Blood* **113**, 1977-1981 (2009).

36 Reina, M. & Espel, E. Role of LFA-1 and ICAM-1 in cancer. *Cancers* **9**, 153 (2017).

37 Kang, M. *et al.* T-Cell-Mimicking Nanoparticles for Cancer Immunotherapy. *Advanced Materials* **32**, 2003368 (2020).

38 Maeda, H. Macromolecular therapeutics in cancer treatment: the EPR effect and beyond. *Journal of Controlled Release* **164**, 138-144 (2012).

39 Ma, J. *et al.* PD1 Hi CD8+ T cells correlate with exhausted signature and poor clinical outcome in hepatocellular carcinoma. *Journal for*

immunotherapy of cancer **7**, 1-15 (2019).

40 Hargadon, K. M., Johnson, C. E. & Williams, C. J. Immune checkpoint blockade therapy for cancer: an overview of FDA-approved immune checkpoint inhibitors. *International immunopharmacology* **62**, 29-39 (2018).

41 Dine, J., Gordon, R., Shames, Y., Kasler, M. K. & Barton-Burke, M. Immune checkpoint inhibitors: an innovation in immunotherapy for the treatment and management of patients with cancer. *Asia-Pacific journal of oncology nursing* **4**, 127 (2017).

42 Hamanishi, J. *et al.* Safety and antitumor activity of anti–PD-1 antibody, nivolumab, in patients with platinum-resistant ovarian cancer. *Journal of Clinical Oncology* **33**, 4015-4022 (2015).

43 Pennock, G. K. & Chow, L. Q. The evolving role of immune checkpoint inhibitors in cancer treatment. *The oncologist* **20**, 812 (2015).

44 Topalian, S. L. *et al.* Safety, activity, and immune correlates of anti–PD-1 antibody in cancer. *New England Journal of Medicine* **366**, 2443-2454 (2012).

45 Cheung, A. S., Zhang, D. K., Koshy, S. T. & Mooney, D. J. Scaffolds that mimic antigen-presenting cells enable ex vivo expansion of primary T cells. *Nature biotechnology* **36**, 160 (2018).

46 Ko, K.-W. *et al.* Attenuation of Tumor Necrosis Factor-α Induced Inflammation by Umbilical Cord-Mesenchymal Stem Cell Derived

Exosome-Mimetic Nanovesicles in Endothelial Cells. *Tissue Engineering and Regenerative Medicine*, 1-9 (2020).

47 Morse, M. A., Gwin, W. R. & Mitchell, D. A. Vaccine Therapies for Cancer: Then and Now. *Targeted Oncology*, 1-32 (2021).

48 Cheever, M. A. & Higano, C. S. PROVENGE (Sipuleucel-T) in prostate cancer: the first FDA-approved therapeutic cancer vaccine. *Clinical Cancer Research* **17**, 3520-3526 (2011).

49 Ye, Z., Qian, Q., Jin, H. & Qian, Q. Cancer vaccine: learning lessons from immune checkpoint inhibitors. *Journal of Cancer* **9**, 263 (2018).

50 Accolla, R. S., Buonaguro, L., Melief, C., Rammensee, H.-G. & Bassani-Sternberg, M. Novel Strategies for Anti-Tumor Vaccines. *Frontiers in immunology* **10**, 3117 (2020).

51 Buonaguro, L. & Tagliamonte, M. Selecting Target Antigens for Cancer Vaccine Development. *Vaccines* **8**, 615 (2020).

52 Schumacher, T. N. & Schreiber, R. D. Neoantigens in cancer immunotherapy. *Science* **348**, 69-74 (2015).

53 Bodey, B., Bodey Jr, B., Siegel, S. E. & Kaiser, H. E. Failure of cancer vaccines: the significant limitations of this approach to immunotherapy. *Anticancer research* **20**, 2665-2676 (2000).

54 Karpanen, T. & Olweus, J. The potential of donor T-cell repertoires in neoantigen-targeted cancer immunotherapy. *Frontiers in immunology* **8**, 1718 (2017).

55 Kaiser, J. (American Association for the Advancement of

Science, 2017).

56 Rosenberg, S. A. & Restifo, N. P. Adoptive cell transfer as personalized immunotherapy for human cancer. *Science* **348**, 62-68 (2015).

57 Kroll, A. V. *et al.* Nanoparticulate delivery of cancer cell membrane elicits multiantigenic antitumor immunity. *Advanced materials* **29**, 1703969 (2017).

58 Fang, R. H. *et al.* Cancer cell membrane-coated nanoparticles for anticancer vaccination and drug delivery. *Nano letters* **14**, 2181-2188 (2014).

59 Bowen, W. S., Svrivastava, A. K., Batra, L., Barsoumian, H. & Shirwan, H. Current challenges for cancer vaccine adjuvant development. *Expert review of vaccines* **17**, 207-215 (2018).

60 Banstola, A., Jeong, J.-H. & Yook, S. Immunoadjuvants for cancer immunotherapy: A review of recent developments. *Acta biomaterialia* (2020).

61 Cuzzubbo, S. *et al.* Cancer Vaccines: Adjuvant Potency, Importance of Age, Lifestyle, and Treatments. *Frontiers in Immunology* **11**, 3850 (2021).

62 Link, B. K. *et al.* Oligodeoxynucleotide CpG 7909 delivered as intravenous infusion demonstrates immunologic modulation in patients with previously treated non-Hodgkin lymphoma. *Journal of Immunotherapy* **29**, 558-568 (2006).

63 Dudek, A. Z. *et al.* First in human phase I trial of 852A, a novel systemic toll-like receptor 7 agonist, to activate innate immune responses in patients with advanced cancer. *Clinical Cancer Research* **13**, 7119-7125 (2007).

64 Choo, Y. W. *et al.* M1 macrophage-derived nanovesicles potentiate the anticancer efficacy of immune checkpoint inhibitors. *Acs Nano* **12**, 8977-8993 (2018).

65 Hong, J. *et al.* T-Cell-Derived Nanovesicles for Cancer Immunotherapy. *Advanced Materials* **33**, 2101110 (2021).

66 Jung, M. *et al.* Nanovesicle-Mediated Targeted Delivery of Immune Checkpoint Blockades to Potentiate Therapeutic Efficacy and Prevent Side Effects. *Advanced Materials* **34**, 2106516 (2022).

67 Van Deursen, J. M. The role of senescent cells in ageing. *Nature* **509**, 439-446 (2014).

68 Crescenzi, E. *et al.* NF-κB-dependent cytokine secretion controls Fas expression on chemotherapy-induced premature senescent tumor cells. *Oncogene* **30**, 2707-2717 (2011).

69 Whiteside, T. L. Tumor-derived exosomes and their role in cancer progression. *Advances in clinical chemistry* **74**, 103-141 (2016).

70 Gu, X., Erb, U., Büchler, M. W. & Zöller, M. Improved vaccine efficacy of tumor exosome compared to tumor lysate loaded dendritic cells in mice. *International journal of cancer* **136**, E74-E84 (2015).

71 Kersten, K., de Visser, K. E., van Miltenburg, M. H. & Jonkers, J. Genetically engineered mouse models in oncology research and cancer medicine. *EMBO molecular medicine* **9**, 137-153 (2017).

72 Jimbu, L. *et al.* Is There a Place for PD-1-PD-L Blockade in Acute Myeloid Leukemia? *Pharmaceuticals* **14**, 288 (2021).

73 Liu, C. *et al.* A nanovaccine for antigen self-presentation and immunosuppression reversal as a personalized cancer immunotherapy strategy. *Nature Nanotechnology*, 1-10 (2022).

74 Xing, Y. & Hogquist, K. A. T-cell tolerance: central and peripheral. *Cold Spring Harbor perspectives in biology* **4**, a006957 (2012).

75 Liu, J. *et al.* Cancer vaccines as promising immuno-therapeutics: Platforms and current progress. *Journal of Hematology & Oncology* **15**, 28 (2022).

76 Liu, H. *et al.* Functional crosstalk between mTORC1/p70S6K pathway and heterochromatin organization in stress-induced senescence of MSCs. *Stem Cell Research & Therapy* **11**, 1-17 (2020).

77 Hsu, C.-H., Altschuler, S. J. & Wu, L. F. Patterns of early p21 dynamics determine proliferation-senescence cell fate after chemotherapy. *Cell* **178**, 361-373. e312 (2019).

78 Hsu, D.-H. *et al.* Exosomes as a tumor vaccine: enhancing potency through direct loading of antigenic peptides. *Journal of immunotherapy* **26**, 440-450 (2003).

79 Admyre, C., Johansson, S. M., Paulie, S. & Gabrielsson, S. Direct

exosome stimulation of peripheral humanT cells detected by ELISPOT. *European journal of immunology* **36**, 1772-1781 (2006).

80 Kim, H. Y. *et al.* Immunomodulatory lipocomplex functionalized with photosensitizer-embedded cancer cell membrane inhibits tumor growth and metastasis. *Nano letters* **19**, 5185-5193 (2019).

81 Schlickeiser, S. *et al.* Control of TNF-induced dendritic cell maturation by hybrid-type N-glycans. *The Journal of Immunology* **186**, 5201-5211 (2011).

82 Gardner, J. K. *et al.* Elderly dendritic cells respond to LPS/IFN-γ and CD40L stimulation despite incomplete maturation. *PLoS One* **13**, e0195313 (2018).

83 Kang, M. *et al.* Nanocomplex-Mediated In Vivo Programming to Chimeric Antigen Receptor-M1 Macrophages for Cancer Therapy. *Advanced Materials* **33**, 2103258 (2021).

국문초록

주요어: 암, 암 면역치료, 나노소포체, T 세포 치료제, 암 백신

학번: 2018-25874

기존 암 치료법과 달리, 암 면역치료는 환자 고유의 면역체계를 이용하여 암을 치료하고자 한다. 대표적인 암 면역치료법으로는 T세포 주입법, 면역관문억제제, 암 백신이 있는데, 실제 암 환자에서 뛰어난 치료 효과를 보여, 암 면역치료제의 가능성을 보여주었다. 하지만 암 면역치료제들은 아직 암의 면역회피 또는 표적선정의 어려움 등의 한계점을 가지고 있어, 수많은 연구들이 계속 진행되고 있다. 이러한 한계점을 극복하기 위해, 세포 유래의 나노소포체를 새로운 암 면역치료제로서 제시하고자 한다. T세포로부터 만들어진 나노소포체 TCNV와 Senescence가 유도된 암세포 유래의 나노소포체 SCCNV는 모세포의 특성을 모두 가지고 있으며, 이를 통해 암 치료를 위한 면역 자극을 일으킬 수 있다는 것을 검증하였다. 또한 이러한 나노소포체의 암 치료효과는 다양한 마우스 암 모델에서 확인하였다. 결론적으로, 세포 유래의 나노소포체는 유망한 암 면역치료제로서의 가능성을 보여주었다.